ANALYSIS OF TURBULENT FLOW IN A PIPE AT CONSTANT REYNOLDS NUMBER USING COMPUTATIONAL FLUID DYNAMICS

BATHSHEBA KERUBO MENGE

DOCTOR OF PHILOSOPHY

(Applied Mathematics)

JOMO KENYATTA UNIVERSITY OF AGRICULTURE AND TECHNOLOGY.

2014

Analysis of Turbulent Flow in a Pipe at Constant Reynolds Number using Computational Fluid Dynamics

Bathsheba Kerubo Menge

A thesis submitted in partial fulfillment for the degree of Doctor of Philosophy in Applied Mathematics in the Jomo Kenyatta University of Agriculture and Technology.

2014

DECLARATION

This thesis is my original work and has not been presented elsewhere for a degree award.

Signature _____ Date_____

Bathsheba Kerubo Menge

This thesis has been submitted for examination with our approval as Universty Supervisors;

Signature_____ Date_____

Prof. Mathew Kinyanjui

J.K.U.A.T, Kenya

Signature_____ Date_____

Prof. Johana Sigey

J.K.U.A.T, Kenya

DEDICATION

This work is dedicated to my father; husband and children: Kimbell, Lyne and Phoebe for giving me easy moments during my studies.

ACKNOWLEDGEMENT

First I would like to express my appreciation to the technical University of Mombasa for financing my studies.

I am greatly indebted to my supervisors Professor Mathew Kinyanjui and Professor Johana Sigey for their patient guidance, understanding and excellent advice during the course of this work. Their friendship and support have not only made the completion of this thesis possible but has left an impression that will continue to influence my work.

My sincere appreciation and special thanks to my Father Mathew Menge, my husband Sam Makori, My children Kimbell, Lyne and Phoebe, my brothers and sisters for their love, support and prayers and for patiently enduring many sacrifices as a result of this dissertation.

I am ever grateful to Almighty God, the creator to whom I owe my very existence.

TABLE OF CONTENTS

LIST OF TABLES

LIST OF FIGURES

NOMENCLATURE

Roman Symbol	Quantity
A	Area, [m^2]
$\vec{A}$	Surface area vector
B	Additive constant
C_1, C_2	Model constants
$C_\mu, C_{1\varepsilon}, C_{2\varepsilon}, C_S$	Model constant parameters for $k-\varepsilon$
C	Dimensionless constant of proportionality
C_p	Pressure coefficient
C_{ij}	Cross-stresses
C_{dym}	Dynamic parameter
C_{SGS}	Smagorinsky constant
D	Diameter of the pipe, [m]
E	Empirical constant
F_c	Blending function
f	Force, [N]

G_k	Kinetic energy, [$m^2 s^{-2}$]
k	von Karman constant
k_P	Turbulence kinetic energy at the near wall node P
L	Length, [m]
L_{ij}	Leonard stresses
N	Number of nodes
P	Pressure
$\overline{p}$	Filtered pressure field
Pr	Prandtl number
Re	Reynolds number
R_{ij}	LES Reynolds stresses
$\vec{r}$	Position vector at the field point
$\vec{r}_w$	Position vector on the wall boundary
S_u, S_v, S_w	Viscous momentum source terms
S_{MX}, S_{MY}, S_{MZ}	Source terms
S_{NX}, S_{NY}, S_{NZ}	Source terms
S_ϕ	Source of ϕ per unit volume

t	Time, [s]
U_P	Mean velocity of the fluid at the near wall node P
u	Inlet velocity of the flow, [ms^{-1}]
u'	Fluctuation velocity, [ms^{-1}]
U, V, W	Velocity components
$\overline{u}, \overline{v}, \overline{w}$	Filtered velocity field
V	Cell volume, [m^{-3}]
ν_t	Kinematic turbulent viscosity, [$m^2 s^{-1}$]
y	Normal distance from the wall at cell centers
$\vec{v}$	Velocity vector, [ms^{-1}]
y^+	Non-dimensional wall distance from the wall
y_P	Distance from point P

Greek symbol	Quantity
α	Thermal diffusivity, [$m^2 s^{-1}$]
β	Coefficient of thermal expansion, [K^{-1}]
$\beta_1, \beta_2, \beta^*$	Model constants for $k-\omega$
γ	Ratio of specific heat
γ_1, γ_2	Model constants
∇	Gradient operator
Δ	Change in variable
∂	Delta function
$\frac{\partial U}{\partial y}$	Mean velocity gradient
ε	Turbulent dissipation, [$m^2 s^{-3}$]
k	Turbulent kinetic energy, [$m^2 s^{-2}$]
ℓ	Turbulent length scale, [m]
ω	Specific dissipation, [s^{-1}]
ρ	Fluid density, [kgm^{-3}]
ϑ	Velocity scale, [ms^{-1}]
μ	Dynamic viscosity, [Nsm^{-2}]

μ_t	Turbulent viscosity, [Nsm^{-2}]
μ_t	High Reynolds-number definition
μ_{SGS}	SGS eddy viscosity
σ	Prandtl number
$\sigma_k, \sigma_\omega, \sigma_{\omega,1}, \sigma_{\omega,2}$	Model constants
τ	**S**hear stress, [Nm^{-2}]
τ_w	Wall shear stress, [Nm^{-2}]
u_τ	Friction velocity
ν_{SGS}	Kinematic SGS viscosity
ϕ	Flow parameter /equivalence ratio
$\bar{\phi}$	Filtered resolved part
ϕ'	Sub-filter unresolved part
ϕ_f	Value of ϕ convected through face f
$\rho f \vec{v}_f \phi_f \cdot \vec{A}_f$	Mass flux through the face
$\vec{A}_f$	Area of face f, $\left\|A\right\|\left(=\left\|A_x\hat{i}+A_y\hat{j}\right\| in\ 2D\right)$

$(\nabla\phi)_n$	Magnitude of $\nabla\phi$ normal to face f
$\nabla\phi$	Gradient of ϕ
Δ	Filter cutoff width.
τ_{ij}	Sub grid scale (SGS) Reynolds Stress
Γ_ϕ	Diffusion coefficient for ϕ
Γ_w	Union of all wall boundaries involved
Φ	Flow parameter
Ψ, ψ	Flow parameters
λ_ε	Blending function

ABBREVIATIONS

CFD	Computational Fluid Dynamics
DES	Detached Eddy Simulation
DNS	Direct Numerical Simulation
EWT	Enhanced Wall Treatment
FVM	Finite Volume Method
LES	Large Eddy Simulation
PDE	Partial Differential Equation
RANS	Reynolds-averaged Navier-Stokes
RSM	Reynolds Stress Model
SGS	Sub-grid Scale Stresses
ske	Standard k-ε
SST	Shear-Stress Transport
TKE	Turbulent Kinetic Energy

ABSTRACT

Computational Fluid Dynamics (CFD) based simulation procedures are considered to be an indispensable analysis and design tool in a wide and ever-increasing range of applications involving fluid flow. This work presents computational investigation of turbulent flow inside pipes of varying diameters. A computational fluid dynamics model of turbulent flow in the pipes is implemented with the help of ANSYS FLUENT 6.3.26 software. Two Reynolds Averaged Navier Stokes Turbulent models; the $k-\varepsilon$ and $k-\omega$ models are used for the simulation and the variation of axial velocity, skin friction coefficient and turbulent intensity along the length of the pipes is analyzed. The viscous boundary layer is expected to grow along the pipe starting at the inlet. It will eventually grow to fill the pipe completely (provided that the pipe is long enough). When this happens, the flow becomes fully-developed and there is no variation of the velocity profile in the axial direction. A closed-form solution to the governing equations can be obtained in the fully-developed region. The fluid used for this purpose is air and the pipe material is aluminium. The Reynold's number is based on the pipe diameter and average velocity at the inlet and is taken as 10,000 for fully turbulent flow. The numerical results obtained from two models are compared with each other and validated against experimental data from the literature. Between the two models, the *k-epsilon* model was found to give better results.

CHAPTER ONE

INTRODUCTION AND LITERATURE REVIEW

1.0 INTRODUCTION

Fluid flow is classified as external or internal depending on whether the fluid is forced to flow over a surface or in a conduit. The transport of fluid in a closed conduit is extremely important in daily operations. There is a wide variety of applications of flow in a pipe. For instance the hot and cold water used in our homes is pumped through pipes. Water in a city is distributed by extensive piping networks. Oil and natural gas are transported hundreds of miles through large pipelines. Blood is transported throughout our bodies by arteries and veins. In an engine, the cooling water is transported by hoses to the pipes in the radiator where it is cooled as it flows. Thermal energy in a hydronic space heating system is transferred to the circulating water in the boiler, and then it is transported to the desired locations through pipes. The analysis of pipe flow is also very important from the engineering point of view.

Due to rigorous engineering application and implications, it is necessary to carry out an analysis on the nature of flow inside pipes and tubes. The objective of the present work is to investigate the nature of fully developed turbulent flow in a pipe computationally and to determine the various parameters such as skin friction coefficient, axial velocity, turbulent intensity and centerline velocity associated with it. The fluid used for this purpose is air with Pr = 0.7.

1.1 Turbulence

Turbulence is a phenomenon of fluid flow that occurs when momentum effects dominate viscous effects high Reynolds number Jurij (2007). Turbulence is characterized by random fluctuating motion of the fluid masses in three dimensions and is characterized by randomly fluctuating velocity fields at many distinct length and time scales. The fluctuating velocity fields manifest themselves as eddies or regions of swirling motion, Wilcox (2004). The free surface flow occurring in nature is almost always turbulent. Turbulent flow is irregular, random and chaotic. The flow consists of a spectrum of different scales (eddy sizes) where largest eddies are of the order of the flow geometry, Launder and Spalding (1972). At the other end of the spectra we have the smallest eddies which are by viscous forces dissipated into internal energy. Turbulent flow is dissipative, which means that kinetic energy in the small (dissipative) eddies are transformed into internal energy. The small eddies receive the kinetic energy from slightly larger eddies. The slightly larger eddies receive their energy from even larger eddies and so on. The largest eddies extract their energy from the mean flow. This process of transferred energy from the largest turbulent scales (eddies) to the smallest is called cascade process.

1.2 Mechanism of internal flow

The fluid body is of finite dimensions and is confined by the pipe walls. At the entry region to a pipe, the fluid develops a boundary layer next to the pipe walls, while the central "core" of the fluid may remain as a uniform flow. Within the boundary layer viscous stresses are very prominent, slowing down the fluid due to

its friction with the pipe walls. This slowdown propagates away from the walls. As the fluid enters the pipe the fluid particles immediately next to the walls are slowed down, these particles then viscously interact with and slow down those in the second layer from the wall, and so on. Downstream, the thickness of this boundary layer increases in the flow direction until the boundary layer reaches the pipe center and thus fills the entire pipe. The region from the pipe inlet to the point at which the boundary layer merges at the centerline is called the hydrodynamic entrance region, and the length of this region is called the hydrodynamic entry length. In the region beyond the entrance region, the velocity profile is fully developed and remains unchanged. The velocity assumes some average profile across the channel which is no longer influenced by any edge effects arising from the entrance region (see Figure 1).

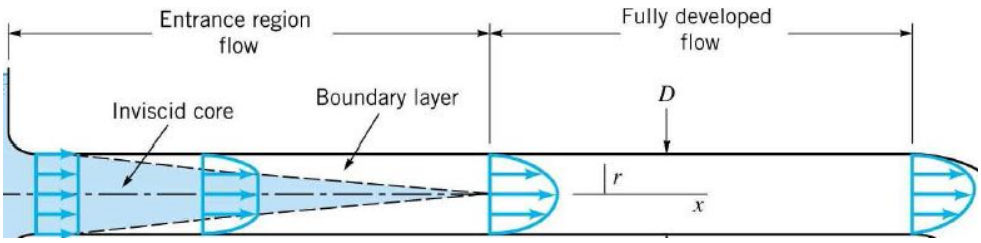

Figure1: Mechanism of internal flow

1.3 Review of Literature

In recent years, a large number of research analyses has been carried out on the internal flows. Taylor (1984) modeled the airflow through sampling pipes. The study found out that for a steady incompressible fluid flow through a smooth pipe, the energy conservation equation can be used. This equation is applicable to either laminar or turbulent flow. Cole (1999) investigated the disturbances to pipe flow regimes by jet induction to improve the available techniques to mathematically model the performance of aspirated smoke detection systems. The study showed that there is a significant area of uncertainty in determining the friction factor. He suggested that the assumption that the flow regime can be regarded as fully developed may not be true. Similar to the work carried out by Taylor (1984), Cole (1999) suggested that the energy losses in any pipe fitting can be broken down into three components: entry loss, exit loss and friction losses. Bloor (1964) investigated the flow around a circular cylinder between Reynolds' number of 200 to 400 when turbulent motion starts to develop in the wake region of the flow. He observed that the transition of flow in the wake region is triggered by large-scale three-dimensional structures.

Several studies have been done on the flow patterns in pipes by Mullin and Peixinho (2006), Sahu *et al* (2009), Willis *et al* (2008). Saho *et al* (2009) investigated the accuracy of numerical modelling of the laminar equation to determine the friction factor of pipe. . They found the friction factor to be 0.0151 at the entrance length of 2.7068m. Banfi *et al* (1981) used a laser-Doppler velocimeter to investigate transitional pipe flow, in particular the behavior of the

velocity fluctuations as the Reynolds number was increased from 1500 to 4000. It was noted that the velocity fluctuations reached a maximum at a Reynolds number of about 2800 (in the transition region). Rudman *et al* (2002) compared results from experimental and numerical investigations of non–Newtonian fluids at transition to turbulence and in weakly turbulent flows. Experimental results showed flow features similar to turbulent puffs and slugs observed in Newtonian transitional flows. Numerical results showed some quantitative discrepancies with the experimental results but did show turbulence suppression, drag reduction and delayed transition as observed experimentally. Yogini (2010) carried out a numerical simulation of flow past a circular cylinder with large eddy simulation (LES) and RANS Shear-Stress Transport (SST) approaches for Reynolds 1000 and 3900. The numerical results extracted from these simulations have good agreement with the experimental data of Zdravkovich (1997).). Analysis of fully developed turbulent flow in a pipe using computational fluid dynamics was carried out by Bhandari D. and Singh S. (2012) and the results obtained computationally were in agreement with analytical results.

The historical overview of the study of turbulence, begins with Leonardo da Vinci in the fifteenth Century. The first turbulence modelling is traced back to his drawings. Boussinesq (1877) introduced the idea of an eddy viscosity in addition to molecular viscosity. The hypothesis that ’turbulent stresses are linearly proportional to mean strain rates’ is still the cornerstone of most turbulence models.

Reynolds' Osborne (1895) experiments led to identification of the Reynolds number as the only physical parameter involved in transition to turbulence in a simple incompressible flow over a smooth surface. Following Reynolds' introduction of the random view of turbulence and proposed use of statistics to describe turbulent flows, essentially all analyses are along these lines. Prandtl (1925) introduced the idea of a mixing length for determining the eddy viscosity. Taylor (1935) was the first researcher to utilize a more advanced level of mathematical rigor, and he introduced formal statistical methods involving correlations, Fourier transforms and power spectra tools for the analysis of homogeneous isotropic turbulence.

Kolmogorov (1941) published three papers that provide some of the most important and most often quoted results of turbulence theory now referred to as the "K41 theory". The K41 theory provides two specific, testable results: the $^{2}/_{3}$ law which leads directly to the prediction of a $K^{-5/3}$ decay rate in the inertial range of the energy spectrum, and the $^{4}/_{5}$ law that is the only exact results for turbulence at high *Re*. Kolmogorov scale is another name for dissipation scales. These scales were predicted on the basis of dimensional analysis as part of the K41 theory. In addition, Kolmogorov (1942) developed the $k-\omega$ concept which provides the turbulent length scale, $\frac{k^{1/2}}{\omega}$ where $^{1}/_{\omega}$ is the turbulent time scale. Prandtl (1945) theorized an eddy viscosity which is dependent on turbulent kinetic energy.

A number of new techniques were introduced beginning in the late 1950s with the work of Kraichnan (1958) who utilized mathematical methods from quantum field theory in the analysis of turbulence. Lorenz (1963) presented a deterministic solution

to a simple model of the Navier-Stokes equations By the beginning of the 1970s attention began to focus on more practical flows such as wall-bounded shear flows (especially boundary-layer transition), flow over and behind cylinders and spheres, jets, plumes, etc. From the standpoint of present-day turbulence investigations the most important advances of the 1970s and 80s were the computational techniques. The first of these was large-eddy simulation (LES) as proposed by Deardorff (1970). This was rapidly followed by the first direct numerical simulation (DNS) by Orszag and Patterson (1972), and introduction of a wide range of Reynolds-averaged Navier–Stokes (RANS) approaches by Launder and Spalding (1972). By the beginning of the 1990s computing power had reached a level to allow consideration of using LES for some practical problems involving sufficiently simple geometry.

Many new approaches are being explored, especially for construction of the required subgrid-scale models. These include the dynamic models of Germano *et al* (1991) and Piomelli (1993). By far the most extensive work on two-equation models has been done by Launder and Spalding (1972). Launder's $k-\varepsilon$ model is the most widely used two-equation model. Launder and Sharma (1974) improved the $k-\varepsilon$ model and called it the standard $k-\varepsilon$ model. The first two-equation $k-\omega$ model was proposed by Kolmogorov (1942). After the initial development, many versions of the $k-\omega$ model were devised with some improvements by Saffman (1970), Wilcox and Alber (1972), Saffman and Wilcox (1974), Wilcox and Traci (1976), Wilcox and Rubesin (1980) and Wilcox (1998), Speziale e*t al* (1990), Menter (1992) and Peng *et al* (1997). The $k-\omega$ model enjoys advantages over the $k-\varepsilon$ model,

especially for integrating through the viscous sub layer and for predicting effects of adverse pressure gradient.

1.4 Statement of the problem

In the studies cited above, one of the problems in fluid mechanics is the determination of the flow field represented by a circular cylinder. The study of wall shear turbulent velocity profiles is a basic subject in fluid mechanics. In particular, the study of turbulent velocity profiles in a pipe is one of the most important subjects in industrial flow applications. In this study we want to investigate the velocity profiles in different pipes and how the pipe diameter affects the velocity profile at a constant Reynolds number.

1.5 General Research objectives

To simulate and assess the performance of two-equation RANS models; $k-\varepsilon$ and $k-\omega$ model in predicting turbulent flow inside pipes of different diameters at a constant Reynolds's number.

1.6 Specific objectives

(i).To computationally investigate the effect of turbulent flow inside pipes of different diameters for two models; $k-\varepsilon$ and $k-\omega$ while maintaining a Reynolds' number at 10,000.

(ii).To investigate the effects of variation of centerline velocity, skin friction coefficient and turbulent intensity along the length of the pipes of different diameters for the two models on velocity profile.

(iii).To establish the relationship between turbulent intensity and axial velocity along pipes of different diameters.

(iv).To obtain the best model for simulating turbulent pipe flow.

1.7 Justification

The flow in circular cylinders has been extensively studied due to its importance in many practical applications, such as fluid in body transport, pipelines, coolers, air conditioning systems, etc. The study of turbulent pipe flow is useful to engineers partly because most flows encountered in engineering practice and in nature are turbulent. Therefore it is a major goal for the industry to understand the fluid behavior and accurately predict the flow regime of fluids. In some situations the velocities in the whole enclosure are important in order to ascertain how flow conditions deviate with varying diameters. Accurate prediction is helpful for the analysis of pipe flow in industrial applications. The outcome of the present study will make a significant contribution to the theory of turbulent pipe flow by identifying the most suitable model for predicting the velocity of flow regime inside a circular pipe.

1.8 Outline

Chapter one briefly introduces the mechanism of internal flow and states the objectives and justification of the work. It also gives the literature review and history of Turbulence.

Chapter two discusses the theoretical background of basic equations describing fluid motion. It explains how CFD formulates these equations. By using those equations, the Navier-Stokes equations are derived. It also gives the definition of turbulence.

In chapter three, the model description is presented. The classification of the models are discussed based on space filtering and time averaging. Different turbulence models such as the LES and the RANS models are explained with the suitability of each model in the applications of the flow in a circular cylinder. The last part of this chapter contains the information about law of the wall.

Chapter four presents the numerical method used to solve the governing equations. It gives an overview of CFD. The method of solution for the overall solution is outlined.

Chapter five presents work done on the flow in pipes of different diameters using RANS $k-\varepsilon$ and $k-\omega$ models at a constant Reynolds number. The results obtained are presented and discussed in this chapter.

Chapter six focuses mainly on the conclusions, recommendations and suggestions for further study based on the objectives of the work. Titles and names of journals where this work has been published are also given.The list of references arranged in alphabetical order by name of the authors is given.

The next chapter presents the equations fundamental to the analysis of fluid flow phenomena.

CHAPTER TWO

GOVERNING EQUATIONS

2.0 Introduction

This chapter gives the general equations governing turbulent fluid flow. The Navier-Stokes equations governing the flow have been used. In mid-18th century, the French engineer Claude Navier and the Irish mathematician George Stokes derived the well-known equations of fluid motion, known as the Navier-Stokes equations. These equations have been derived based on the fundamental governing equations of fluid dynamics, called the continuity, the momentum and the energy equations, which represent the conservation laws of physics, Anderson (1995).

2.1 Continuity equation

The equation of continuity also known as the equation of conservation of mass is derived based on two fundamental principles namely;

i). that the rate of increase of mass in fluid element is equal to the net rate of flow of mass into the fluid element, White (1974);

ii).The continuum hypothesis which states that there are no empty spaces between particles that were in contact and that the fluid volume is not affected by an increase in pressure, that is, the flow is continuous.

The equation can be expressed as:

$$\frac{\partial \rho}{\partial t} + \frac{\partial (\rho u)}{\partial x} + \frac{\partial (\rho v)}{\partial y} + \frac{\partial (\rho w)}{\partial z} = 0 \qquad (2.1)$$

or in vector notation

$$\frac{\partial \rho}{\partial t} + div(\rho u) = 0 \qquad (2.2)$$

Equation (2.2) is the unsteady, three-dimensional mass conservation or continuity equation at a point in a compressible fluid, Versteeg and Malalasekera (2007).

For an incompressible fluid the density is constant and equation (2.2) becomes

$$div\ u = 0 \qquad (2.3)$$

2.2 Momentum equation

Equation of conservation of momentum is derived from Newton's second law of motion which states that the net rate of momentum must be equal to the net forces acting on the fluid particle, Versteeg and Malalasekera (2007)

The rates of increase of x-, y- and z-momentum are given by

$$\rho \frac{Du}{Dt} = \frac{\partial (-p + \tau_{xx})}{\partial x} + \frac{\partial \tau_{yx}}{\partial y} + \frac{\partial \tau_{zx}}{\partial z} + S_{Mx} \qquad (2.4)$$

$$\rho \frac{Dv}{Dt} = \frac{\partial \tau_{xy}}{\partial x} + \frac{\partial\left(-p + \tau_{yy}\right)}{\partial y} + \frac{\partial \tau_{zy}}{\partial z} + S_{My} \tag{2.5}$$

$$\rho \frac{Dw}{Dt} = \frac{\partial \tau_{xz}}{\partial x} + \frac{\partial\left(-p + \tau_{zz}\right)}{\partial z} + \frac{\partial \tau_{yz}}{\partial y} + S_{Mz} \tag{2.6}$$

2.3 Navier-Stokes equations for a Newtonian fluid

The most useful forms of the conservation equation for fluid flows are obtained by introducing a suitable model for the viscous stresses τ_{ij}. In many fluid flows the viscous stresses can be expressed as functions of the local deformation rate or strain rate, Versteeg and Malalasekera (2007). In three dimensional flows, the local rate of deformation is composed of the linear deformation rate and the volumetric deformation rate. The rate of linear deformation of a fluid element has nine components in three dimensions, six of which are independent in isotropic fluid. They are denoted by the symbol s_{ij}.In a Newtonian fluid the viscous stresses are proportional to the rates of deformation White (1974).

The Navier-stokes equations can be written as

$$\rho \frac{Du}{Dt} = -\frac{\partial p}{\partial x} + div\left(\mu \; grad \; u\right) + S_{Nx} \tag{2.7}$$

$$\rho \frac{Dv}{Dt} = -\frac{\partial p}{\partial y} + div\left(\mu \; grad \; v\right) + S_{Ny} \tag{2.8}$$

$$\rho \frac{Dw}{Dt} = -\frac{\partial p}{\partial z} + div(\mu \ grad \ w) + S_{Nz} \qquad (2.9)$$

Here the source terms S_{Nx}, S_{Ny}, and S_{Nz} in the above equations include contributions due to body forces. By solving these equations, the pressure and velocity of the fluid can be predicted throughout the flow.

To obtain the equations that govern the current problem, the following assumptions are made for the analysis:

(i). steady flow

(ii). Constant transport properties of fluid

(iii). Incompressible fluid flow

(iv). Newtonian fluid

(v). continuum fluid.

Turbulent models may be computed using several approaches: either by solving RANS equations with suitable models for turbulent quantities or by computing them directly. The main approaches are summarized in the next chapter.

CHAPTER THREE

MATHEMATICAL FORMULATION

3.0 Overview

The equations presented in chapter two are general and can be applied to most fluid flow problems. However, before solving these equations a specific problem is posed and boundary conditions for the numerical procedure are presented.

3.1 Model description

In this chapter the set-up of a two-dimensional turbulent fluid flow in a pipe using fluent is illustrated.

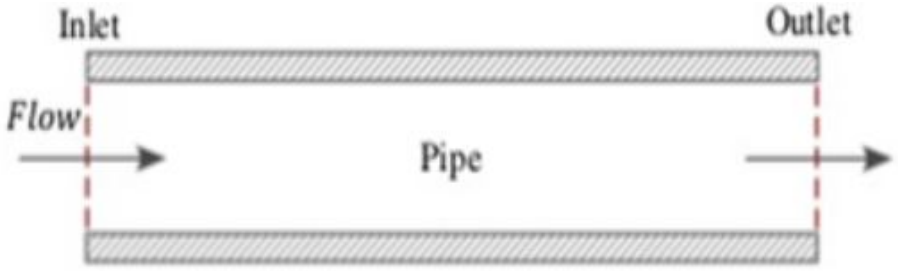

Figure 3.1: Geometry of the problem.

Consider fluid (air) flowing through a circular pipe of varying diameters as illustrated in figure 3.1 above and a length of 20 m. The geometry is symmetric therefore only half portion of the pipe is modelled. Air enters from the inlet boundary with a constant velocity of 1 m/s, density $\rho = 1\ kg/m^3$ and coefficient

of viscosityμ (depending on pipe diameter).The fluid exhausts into the ambient atmosphere which is at a pressure of 1 atm. The Reynolds number based on the pipe diameter and average velocity at the inlet is:

$$Re = \frac{\rho u D}{\mu} = 10000$$

where u is the average velocity at the inlet, which is 1 m/s in this case, D is the pipe diameter, ρ is the density and μ the fluid viscosity. At this Reynolds number, the flow is usually completely turbulent.

Turbulent flows may be computed using several different approaches. Either by solving the Reynolds-averaged Navier-Stokes equations with suitable models for turbulent quantities or by computing them directly. The main approaches are summarized below.

3.2 Classification of Turbulence models.

Turbulent flows are characterized by velocity fields which fluctuate rapidly both in space and time. Since these fluctuations occur over several orders of magnitude it is computationally very expensive to construct a grid which directly simulates both the small scale and high frequency fluctuations for problems of practical engineering significance. Two methods can be used to eliminate the need to resolve these small scales and high frequencies: Filtering and Time averaging Jones and Clarke (2008)

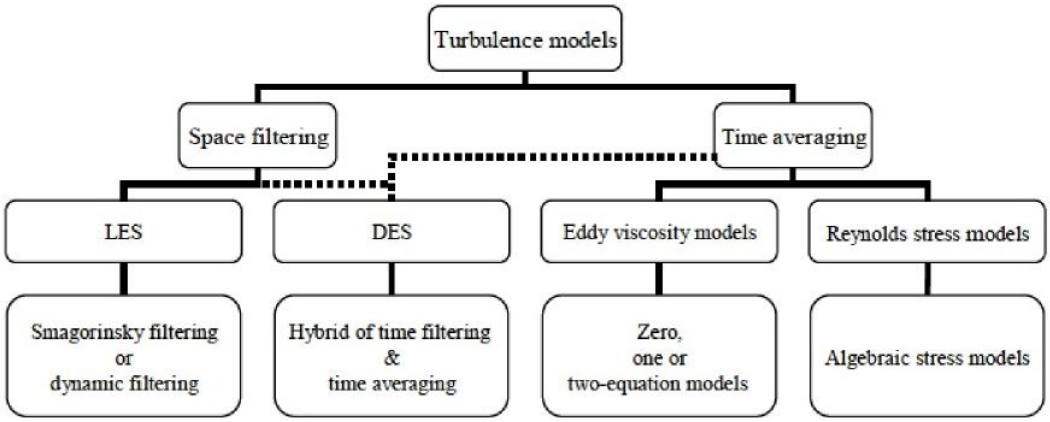

Figure 3.2 (a): Turbulence models classification

Figure 3.2 (a) presents the overview of turbulence models commonly available in CFD. Generally, simulations of flow can be done by filtering or averaging the Navier-Stokes equations.

3.2.1 Space Filtering

The main idea behind this approach is to filter the time-dependent Navier-Stokes equation in either Fourier space or configuration space. A simulation using this approach is known as a Large Eddy Simulation (LES).The filtering process creates additional unknown terms which must be modeled in order to provide closure to the set of equations. These terms are the sub-grid scale stresses and several models for these stresses. The simplest of these is the model originally proposed by Smagorinsky (1963) in which the sub-grid scale stresses (SGS) are computed using an isotropic eddy viscosity approach. The eddy viscosity is then

calculated from an algebraic expression involving the product of a model constant C_S, the modulus of the rate of strain tensor, and an expression involving the filter width. The problem with this approach is that there is no single value of the constant C_S which is universally applicable to a wide range of flows, Jones and Clarke (2008).

3.2.2 Time averaging

In the Time averaging or Reynolds averaging approach all flow variables are divided into a mean component and a rapidly fluctuating component and then all equations are time averaged to remove the rapidly fluctuating components. In the Navier-Stokes equation the time averaging introduces new terms which involve mean values of products of rapidly varying quantities. These new terms are known as the Reynolds Stresses, and solution of the equations initially involves the construction of suitable models to represent these Reynolds Stresses, Wilcox (2004). There are two sub categories for time averaging approach: Eddy-viscosity models (EVM) and Reynolds stress models (RSM).

3.2.3 Eddy-viscosity models

One assumes that the turbulent stress is proportional to the mean rate of strain. Furthermore eddy viscosity is derived from turbulent transport equations (usually *k* plus one other quantity).

- **Zero equation model**: - The mixing length model is a zero equation models based on Reynolds averaged Navier-Stokes equations. It is one of the oldest turbulence model which was developed in the beginning of this century. We assume the kinematic turbulent viscosity ν_t, which can be expressed as a product of a turbulent velocity scale ϑ and a turbulent length scale ℓ, Zevenhoven (2009).

$$\nu_t = C\vartheta\ell \tag{3.1}$$

where C is a dimensionless constant of proportionality. And the dynamics turbulent viscosity is given by

$$\mu_t = C\rho\vartheta\ell$$

The kinetic energy of turbulence is contained in the largest eddies and turbulence length scale ℓ. For such flows it is correct to state that, if the eddy length scale is ℓ ,

$$\vartheta = c\ell\left|\frac{\partial U}{\partial y}\right| \tag{3.2}$$

Where c is a dimensionless constant and $\frac{\partial U}{\partial y}$ is the mean velocity gradient. Combining equations (3.1) and (3.2) and absorbing the two constants C and c into a new length scale ℓ_m we obtain

$$\nu_t = \ell_m^2\left|\frac{\partial U}{\partial y}\right| \tag{3.3}$$

This is Prandtl's mixing length model. This model is easy to implement and cheap in terms of computing resources. Also it is good to predict thin shear layers like jets, mixing layers, wakes and boundary layers. The mixing length model is completely incapable of describing flows with separation and recirculation. It only calculates mean flow properties and turbulent shear stress.

One equation models: - The Spalart-Allmaras model is one equation turbulence model because it solve a single transport equation that determines the turbulent viscosity. This is in contrast to many of the early one-equation models that solve an equation for the transport of turbulent kinetic energy and require an algebraic prescription of a length scale. The Spalart-Allmaras model also allows for reasonably accurate predictions of turbulent flows with adverse pressure gradients. Furthermore, it is capable of smooth transition from laminar to turbulent flow at user specified locations. The Spalart-Allmaras model is an empirical equation that models production, transport, diffusion and destruction of the turbulent viscosity, Blazek (2001). The Spalart-Allmaras model is suitable for aerospace applications involving wall-bounded flows and in the turbo machinery applications. In complex geometries it is difficult to define the length scale, so the model is unsuitable for more general internal flows.

Two equation models: - Two equation turbulence models are one of the most common type of turbulence models. Models like the $k-\varepsilon$ model and the $k-\omega$ model have become industry standard models and are commonly used for most types of engineering problems. By definition, two equation models include two extra

transport equations to represent the turbulent properties of the flow. One of the transported variables is the turbulent kinetic energy, and the second transport variable varies depending on what type of two-equation model it is. Common choices are the turbulent dissipation ε or the specific dissipation ω, Wilcox (2004).

3.2.4 Reynolds stress models

The Reynolds stress model (RSM) is the most elaborate type of turbulence model. The RSM closes the Reynolds-averaged Navier-Stokes equations by solving transport equations for the Reynolds stresses, together with an equation for the dissipation rate. This means that five additional transport equations are required in 2D flows, in comparison to seven additional transport equations solved in 3D. Since the RSM accounts for the effects of streamline curvature, swirl, rotation, and rapid changes in strain rate in a more rigorous manner than one-equation and two-equation models, it has greater potential to give accurate predictions for complex flows, ANSYS FLUENT 12.1 Theory Guide, (2010).

Extent of modeling for certain CFD approaches for turbulence are illustrated in Figure 3.2 (b). It is clearly seen that the DNS and the LES models are computing fluctuation quantities resolve shorter length scales than models solving RANS equations. Hence they have the ability to provide better results. However they have a demand of much greater computer power than those models applying RANS methods Bell, (2003).

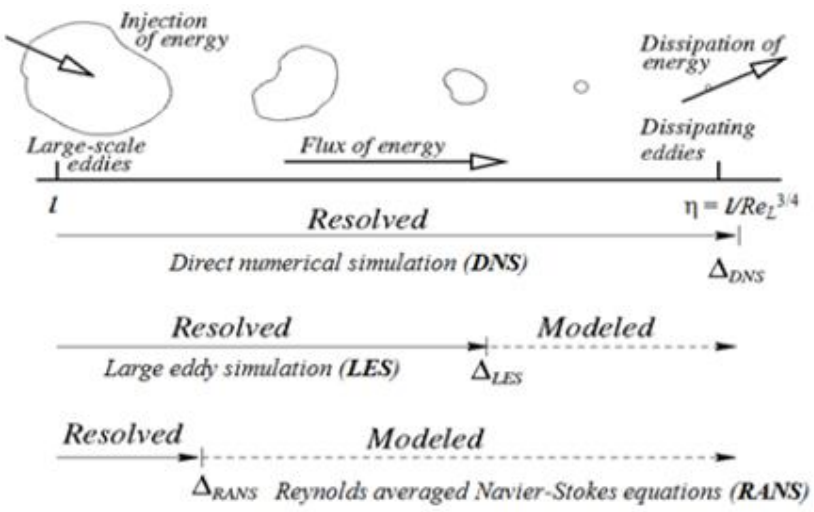

Figure 3.2 (b): Extend of modelling for certain types of turbulence models

3.3 Reynolds averaged Navier-Stokes equations

The basic tool required for the derivation of the Reynolds-averaged Navier-Stokes (RANS) equations from the instantaneous Navier–Stokes equations is the Reynolds decomposition. Reynolds decomposition refers to separation of the flow variables into the mean component and the fluctuating component. The following rules which govern time averages of fluctuating properties $\phi = \Phi + \phi'$ and $\psi = \Psi + \psi'$ and their summation, derivatives and integrals will be useful while deriving the RANS equations:

$$\overline{\phi'} = \overline{\psi'} = 0 \quad \overline{\Phi} = \phi \quad \frac{\overline{\partial \phi}}{\partial s} = \frac{\partial \Phi}{\partial s} \quad \overline{\int \phi ds} = \int \Phi ds$$
$$\overline{\phi + \psi} = \Phi + \Psi \quad \overline{\phi\psi} = \Phi\Psi + \overline{\phi'\psi'} \quad \overline{\phi}\overline{\Psi} = \Phi\Psi \quad \overline{\phi'}\overline{\Psi} = 0 \tag{3.4}$$

In addition, *div* and *grad* are both differentiations, the above rules can be extended to a fluctuating quantity $a = A + a'$ and its combinations with a fluctuating scalar $\phi = \Phi + \phi'$, ANSYS FLUENT 12.1 Theory Guide, (2010).

$$\begin{aligned} &\overline{div\ a} = div\ A; \quad \overline{div(\phi a)} = div(\phi a) = div(\Phi A) + div(\phi' a'); \\ &\overline{div\ grad\phi} = div\ grad\ \Phi \end{aligned} \tag{3.5}$$

Consider the instantaneous continuity and Navier-Stokes equations in a Cartesian co-ordinate system so that the velocity vector U has x-component *u*, y-component *v* and z-component *w:*

$$div\, u = 0 \tag{3.6}$$

$$\frac{\partial u}{\partial t} + div(uU) = -\frac{1}{\rho}\frac{\partial p}{\partial x} + div(\mu\ grad(u)) \tag{3.7}$$

$$\frac{\partial v}{\partial t} + div(vU) = -\frac{1}{\rho}\frac{\partial p}{\partial y} + div(\mu\ grad(v)) \tag{3.8}$$

$$\frac{\partial w}{\partial t} + div(wU) = -\frac{1}{\rho}\frac{\partial p}{\partial z} + div(\mu\ grad(w)) \tag{3.9}$$

This system of equations governs every turbulent flow, but the effect of fluctuations on the mean flow using the Reynolds decomposition in equations (3.6), (3.7), (3.8) and (3.9) and replacing the flow variables U and p by the sum of a mean and fluctuating component gives;

$$u = U + u' \quad v = V + v' \quad w = W + w' \quad p = P + p'$$

Then the time average is taken, applying the rules stated in equations (3.6) and (3.7). Considering the continuity equation (3.8), $\overline{div\, u} = div\, U$. This yields the continuity equation for the mean flow:

$$div\, U = 0 \tag{3.10}$$

A similar process is applied on the x-momentum equation (3.9). The time averages of the individual terms in this equation can be written as follows:

$$\overline{\frac{\partial u}{\partial t}} = \frac{\partial U}{\partial t}, \quad \overline{\partial(uU)} = div(uU) + div\left(\overline{u'v}\right)$$
$$\overline{-\frac{1}{\rho}\frac{\partial p}{\partial x}} = -\frac{1}{\rho}\frac{\partial p}{\partial x}, \quad \overline{div(\mu\, grad(u))} = div(\mu\, grad(U))$$

Substitution of these results gives the time-average x-momentum equation

$$\frac{\partial U}{\partial t} + div(uU) + div(u'v') = -\frac{1}{\rho}\frac{\partial P}{\partial x} + div(\mu\, grad(U)) \tag{3.11}$$

Repetition of this process on equations (3.8) and (3.9) yields the time-average y- and z-momentum equations:

$$\frac{\partial V}{\partial t} + div(vU) + div(v'u') = -\frac{1}{\rho}\frac{\partial P}{\partial y} + div(\mu\, grad(V)) \tag{3.12}$$

$$\frac{\partial W}{\partial t} + div(wU) + div(w'u') = -\frac{1}{\rho}\frac{\partial P}{\partial z} + div(\mu\, grad(W)) \tag{3.13}$$

The process of time averaging has introduced new terms (the third terms) in the resulting time-average momentum equations. These terms are a product of fluctuating velocities and are associated with convective momentum transfer due to turbulent eddies. Putting these terms on the right hand side of equations (3.11), (3.12) and (3.13) reflects their role as additional turbulent stresses on the mean velocity components U, V and W:

$$\frac{\partial U}{\partial t} + \mathrm{div}(U\mathbf{U}) = -\frac{1}{\rho}\frac{\partial P}{\partial x} + \nu\ \mathrm{div}\ (\mathrm{grad}(U)) + \frac{1}{\rho}\left[\frac{\partial(-\rho\overline{u'^2})}{\partial x} + \frac{\partial(-\rho\overline{u'v'})}{\partial y} + \frac{\partial(-\rho\overline{u'w'})}{\partial z}\right] \tag{3.14}$$

$$\frac{\partial V}{\partial t} + \mathrm{div}(V\mathbf{U}) = -\frac{1}{\rho}\frac{\partial P}{\partial y} + \nu\ \mathrm{div}\ (\mathrm{grad}(V)) + \frac{1}{\rho}\left[\frac{\partial(-\rho\overline{u'v'})}{\partial x} + \frac{\partial(-\rho\overline{v'^2})}{\partial y} + \frac{\partial(-\rho\overline{v'w'})}{\partial z}\right] \tag{3.15}$$

$$\frac{\partial W}{\partial t} + \mathrm{div}(W\mathbf{U}) = -\frac{1}{\rho}\frac{\partial P}{\partial z} + \nu\ \mathrm{div}\ (\mathrm{grad}(W)) + \frac{1}{\rho}\left[\frac{\partial(-\rho\overline{u'w'})}{\partial x} + \frac{\partial(-\rho\overline{v'w'})}{\partial y} + \frac{\partial(-\rho\overline{w'^2})}{\partial z}\right] \tag{3.16}$$

The extra stress terms have been written out as follows. They result from six additional stresses among of three normal stresses

$$\tau_{xx} = -\rho\overline{u'^2}\ ,\ \tau_{yy} = -\rho\overline{v'^2}\ ,\ \tau_{zz} = -\rho\overline{w'^2} \tag{3.17}$$

and three shear stresses

$$\tau_{xy} = \tau_{yx} = -\rho\overline{u'v'}\ ,\ \tau_{xz} = \tau_{zx} = -\rho\overline{u'w'}\ ,\ \tau_{yz} = \tau_{zy} = -\rho\overline{v'w'} \tag{3.18}$$

These extra turbulent stresses are called the Reynolds stresses. The normal stresses involve the respective variances of the x-, y- and z-velocity fluctuations. They are always non-zero because they contain squared velocity fluctuations Wilcox (2004). The shear stresses contain second moments associated with correlations between different velocity components, Wilcox (2004). If two fluctuations velocity components, e.g. u' and v' are independent random fluctuations, the time average $\overline{u'v'}$ would be zero. The equation set (3.10), (3.14), (3.15) and (3.16) is called the Reynolds-averaged Navier-Stokes equations.

3.3.1 Standard $k-\varepsilon$ model

The Standard $k-\varepsilon$ model, Launder and Spalding (1974) is the most widely used complete RANS model and it is incorporated in most commercial CFD codes, Tannehill *et al* (1997). In this model, the model transport equations are solved for two turbulence quantities i.e. k and ε.

The $k-\varepsilon$ turbulence model solves the flow based on the assumption that the rate of production and dissipation of turbulent flows are in near-balance in energy transfer,

Ferrey and Aupoix (2006). k and ε is used to define velocity scale ϑ and length scale ℓ representative of the large scale turbulence as follows:

$$\vartheta = k^{1/2} \qquad \ell = \frac{k^{3/2}}{\varepsilon}$$

where k is turbulent kinetic energy and ε is the dissipation of turbulent kinetic energy. This is then related to the turbulent viscosity μ_t based on the Prandtl mixing length model, ANSYS FLUENT 12.1 Theory Guide, (2010).

$$\mu_t = C\rho\vartheta\ell = \rho C_\mu \frac{k^2}{\varepsilon} \tag{3.19}$$

The governing transport equations for k and ε of the standard k - ε model are as follows:

$$\frac{\partial(\rho k)}{\partial t} + div(\rho k U) = div\left[\frac{\mu_t}{\sigma_k} grad\, k\right] + 2\mu_t S_{ij} \cdot S_{ij} - \rho\varepsilon \tag{3.20}$$

$$\frac{\partial(\rho \varepsilon)}{\partial t} + div(\rho \varepsilon U) = div\left[\frac{\mu_t}{\sigma_\varepsilon} grad\, \varepsilon\right] + C_{1\varepsilon}\frac{\varepsilon}{k} 2\mu_t S_{ij} \cdot S_{ij} - C_{2\varepsilon}\rho\frac{\varepsilon^2}{k} \tag{3.21}$$

where the first term denotes the rate of change of k or ε. The second and third terms display the transport of k or ε by convection and diffusion respectively, Versteeg and Malalasekera (2007). The last two terms describe the rate of production and destruction of k or ε respectively.

Physically, the rate of change of kinetic energy in equation (3.20) is related to the convection and diffusion of the mean motion of the flow. The diffusion term can be modeled by the gradient diffusion assumption as turbulent momentum transport is assumed to be proportional to mean gradients of velocity. The production term, which is responsible for the transfer of energy from the mean flow to the turbulence, is counterbalanced by the interaction of the Reynolds stresses and mean velocity gradient. The destruction term deals with the dissipation of energy into heat due to viscous nature of the flow Zevenhoven Ron (2009).The equations (3.19) to (3.21) contains five adjustable constants: $C_{\mu}, \sigma_k, \sigma_{\varepsilon}, C_{1\varepsilon}, and\ C_{2\varepsilon}$. Based on extensive examination of a wide range of turbulent flows, the constant parameters used in the equations take the following values;

$$C_{\mu} = 0.09; \quad \sigma_k = 1.00; \quad , \sigma_{\varepsilon} = 1.30; \quad , C_{1\varepsilon} = 1.44; \quad and \quad C_{2\varepsilon} = 1.92 \qquad (3.22)$$

where Prandtl numbers $\sigma_k\ and\ \sigma_{\varepsilon}$ connect to diffusivities of $k\ and\ \varepsilon$. According to ANSYS FLUENT 12.1 Theory Guide (2010), the standard $k-\varepsilon$ model has gained popularity among RANS models due to the following;

Robust formulation, it is one of the earliest two-equation models widely documented, reliable and affordable, has lower computational overhead and excellent performance for many industrially relevant flows. However, the model encounters some difficulties in failing to resolve flows with large strains such as swirling flows and curved boundary layers flow. It also has poor performance in rotating flows.

3.3.2 Standard $k-\omega$ model

Wilcox (1988) developed the standard $k-\omega$ two-equation model. The standard $k-\omega$ model is very similar in structure to the $k-\varepsilon$ model but the variable ε is replaced by the dissipation rate per unit kinetic energy ω. The length scale is $\ell = \sqrt{k}/\omega$, Wilcox (2004). The eddy viscosity is given as;

$$\mu_t = \rho k/\omega \tag{3.23}$$

The transport equations for k *and* ω in standard $k-\omega$ model are

$$\frac{\partial(\rho k)}{\partial t} + div(\rho k U) = div\left[\left(\mu + \frac{\mu_t}{\sigma_k}\right) grad(k)\right] + P_k - \beta^* \rho k \omega \tag{3.24}$$

where $P_k = \left(2\mu_t S_{ij} \cdot S_{ij} - \frac{2}{3}\rho k \frac{\partial U_i}{\partial x_j}\delta_{ij}\right)$

$$\frac{\partial(\rho \omega)}{\partial t} + div(\rho \omega U) = div\left[\left(\mu + \frac{\mu_t}{\sigma_\omega}\right) grad(\omega)\right] + \gamma_1 P_\omega - \beta_1 \rho k \omega^2 \tag{3.25}$$

where $P_\omega = \left(2\rho S_{ij} \cdot S_{ij} - \frac{2}{3}\rho \omega \frac{\partial U_i}{\partial x_j}\delta_{ij}\right)$

where term the first term denotes the rate of change of k *or* ω in the both equation (3.24) and equation (3.25). In addition, the second and third terms display the transport of k *or* ω by convection and diffusion respectively, Wilcox

(2004). The fifth and sixth terms describe the rate of production and destruction of k *or* ω respectively.

The model constants are as follows;

$$\sigma_k = 2.0; \quad \sigma_\omega = 2.0; \quad \gamma_1 = 0.533; \quad \beta_1 = 0.075 \quad and \quad \beta^* = 0.09 \tag{3.26}$$

The replacement with the variable ω allows better treatment in solving the flow near wall. Near to the wall, the boundary layer is affected by viscous nature of the flow. A very refined mesh is necessary to appropriately resolve the flow, ANSYS FLUENT 12.1 Theory Guide, (2010). Although the near wall treatment of standard $k-\varepsilon$ model saves a vast amount of computer power, it is not sufficient to represent complex flow accurately. In the standard $k-\omega$ formulation, the flow near wall is resolved directly through the integration of the ω equation. The advantage of the standard $k-\omega$ model compared to the standard $k-\varepsilon$ model is that the ω equation is more robust and easier to integrate compared to the ε equation without the need of additional damping functions.

3.3.3 Shear-Stress Transport (SST) $k-\omega$ model

The Shear-Stress Transport (SST) $k-\omega$ model was developed to effectively blend the robust and accurate formulation of the $k-\omega$ model in the near-wall region with the free-stream independence of the $k-\varepsilon$ model in the far field, Menter (1994). To achieve this, the $k-\varepsilon$ model is converted into a $k-\omega$ formulation, ANSYS FLUENT 12.1 Theory Guide, (2010). The SST $k-\omega$

model is similar to the standard $k-\omega$ model, but includes the following refinements:

The standard $k-\omega$ model and the transformed $k-\varepsilon$ model are both multiplied by a blending function and both models are added together. The blending function is designed to be one in the near-wall region, which activates the standard $k-\omega$ model, and zero away from the surface, which activates the transformed $k-\varepsilon$ model. The SST model incorporates a damped cross-diffusion derivative term in the ω equation. The definition of the turbulent viscosity is modified to account for the transport of the turbulent shear stress and the modelling constants are different.

The Reynolds stress computational and the *k* equation are the same as in standard $k-\omega$ model, but the ε equation is transformed into an ω equation by substituting $\varepsilon = k\omega$. This yields

$$\frac{\partial(\rho\omega)}{\partial t} + div(\rho\omega U) = div\left[\left(\mu + \frac{\mu_t}{\sigma_{\omega,1}}\right) grad(\omega)\right] + \gamma_2\left(2\rho S_{ij.}S_{ij} - \frac{2}{3}\rho\omega\frac{\partial U_i}{\partial x_j}\delta_{ij}\right)$$
$$-\beta_2\rho\omega^2 + 2\frac{\rho}{\sigma_{\omega,2}\omega}\frac{\partial k}{\partial x_k}\frac{\partial \omega}{\partial x_k}$$

(3.27)

These terms are same as those in equation (3.25) in standard $k-\omega$ model except the last term. The last term is called the cross-diffusion term, which arises during the

$\varepsilon = k\omega$ transformation of the diffusion term in the ε equation, Versteeg and Malalasekera (2007). The model constants are as follows;

$$\sigma_k = 1.0; \quad \sigma_{\omega,1} = 2.0; \quad \sigma_{\omega,2} = 1.17 \quad \gamma_2 = 0.44; \quad \beta_2 = 0.083 \quad and \quad \beta^* = 0.09 \tag{3.28}$$

Here, blending functions are used to achieve a smooth transition between standard $k-\omega$ and transformed $k-\varepsilon$ models. Blending functions are introduced in the equation to modify the cross-diffusion term and are also used for model constants that take value C_1 for the original $k-\omega$ model and value C_2 in Menter's transformed $k-\varepsilon$ model.

$$C = F_c C_1 + (1 - F_c) C_2 \tag{3.29}$$

where F_c is the blending function. The functional form of F_c is chosen so that it is zero at the wall, tends to unity in the far field and produces a smooth transition around a distance half way between the wall and edge of the boundary layer, Versteeg and Malalasekera (2007). The SST $k-\omega$ model is more accurate and reliable for a wider class of flows like, adverse pressure gradient flows, airfoils, transonic shock waves than the standard $k-\omega$ model, Menter (1994).

3.4 The law of the wall

Turbulent flows are significantly affected by the presence of walls. Obviously, the mean velocity field is affected through the no-slip condition that has to be satisfied at

the wall. However, the turbulence is also changed by the presence of the wall in non-trivial ways. Close to the wall the flow is influenced by viscous effects and does not depend on free stream parameters. The mean flow velocity only depends on the distance *y* from the wall, fluid density ρ and viscosity μ and the wall shear stress τ_w , Wilcox (2004).

So

$$U = f(y, \rho, \mu, \tau_w)$$

Dimensional analysis shows that

$$u^+ = \frac{U}{u_\tau} = f\left(\frac{\rho \mu_\tau y}{\mu}\right) = f\left(y^+\right) \tag{3.30}$$

Equation (3.30) is called the law of the wall and contains the definitions of two important dimensionless groups u^+ and y^+. Here $u_\tau = \sqrt{\tau_w / \rho}$ is called friction velocity.

The $k - \varepsilon$ models, the RSM, and the LES model are primarily valid for turbulent core flows and will not predict correct near-wall behavior if integrated down to the wall. Therefore, it is necessary to make these models suitable for wall-bounded flows. The Spalart-Allamas and $k - \omega$ models were designed to be applied throughout the boundary layer, provided that the near-wall mesh resolution is

sufficient. Numerous experiments have shown that the near-wall region can be largely subdivided into three layers.

1. Linear or viscous sub-layer:- the fluid layer in contact with a smooth wall

At the solid surface the fluid is stationary. Turbulent eddying motions must stop very close to the wall and the behavior of the fluid closest to the wall is dominated by viscous effects. The viscous sub-layer is in practice extremely thin ($y^+ < 5$) and assume that the shear stress is approximately constant and equal to the wall shear stress τ_w. After some simple algebra and making use of the definitions of u^+ and y^+ this leads to

$$u^+ = y^+ \tag{3.31}$$

Due to the linear relationship between velocity and distance from the wall, the fluid layer adjacent to the wall is also known as the linear sub-layer.

2. Log-law layer: - the turbulent region close to a smooth wall

Outside the viscous sublayer a region exists where viscous and turbulent effects are both important. The shear stress τ varies slowly with distance from the wall, Wilcox (2004) and within this inner region it is assumed to be constant and equal to the wall shear stress.

Relationship between u^+ and y^+ that is dimensionally correct is given by:

$$u^+ = \frac{1}{k} In\left(y^+\right) + B = \frac{1}{k} In\left(Ey^+\right) \tag{3.32}$$

Here, Von karman's constant k = 0.4 and the additive constant B = 5.5 or (E = 9.8) for smooth wall, wall roughness cause a decrease in the value of B. The value of k and B are universal constants valid for all turbulent flows past smooth walls at high Reynolds number. Equation (3.32) is often called the log-law, and the layer where y^+ takes values between 30 and 500 is the log-law layer.

3. Outer layer: - the inertia-dominated region far from the wall

Experimental measurements show that the log-law is valid in the region $0.02 < y/\delta < 0.2$. For larger values of y the velocity-defect law provides the correct form, ANSYS FLUENT 12.1 Theory Guide, (2010). In the overlap region the log-law and velocity-defect law have to equal and overlap is obtained by assuming the following logarithmic form:

$$\frac{U_{\max} - U}{u_t} = -\frac{1}{k} In\left(\frac{y}{\delta}\right) + A \tag{3.33}$$

where A is a constant. The velocity-defect law is often called the *law of the wake*.

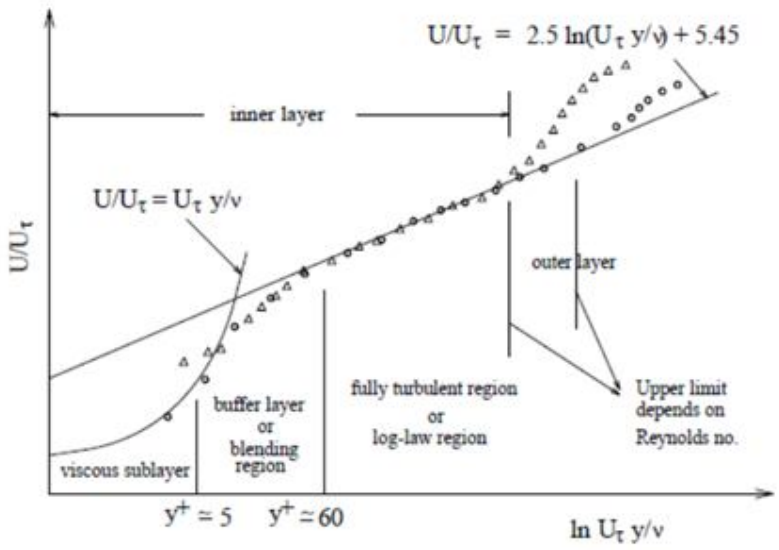

Figure 3.3: Subdivisions of the Near-Wall region.

From Fig.3.3 we can say that the turbulent boundary layer adjacent to a solid surface is composed of two regions, Versteeg and Malalasekera (2007):

(a).The inner region: 10-20% of the total thickness of the wall layer; the shear stress is constant and equal to the wall shear stress τ_w. Within this region there are three zones: the linear sub-layer: viscous stresses dominate the flow adjacent to surface, the buffer layer: viscous and turbulent stresses are of similar magnitude, the log-law layer: turbulent stresses dominate.

(b).The outer region or law-of-the-wake layer: inertia-dominated core flow far from wall; free from direct viscous effects.

In the next chapter, the numerical method used to solve the governing equations is presented. The principles of CFD and brief details of the simulation are discussed.

CHAPTER FOUR

METHODOLOGY.

4.0 INTRODUCTION.

Flow in pipes has been the subject of both experimental and numerical studies for decades. This flow is very sensitive to the changes of Reynolds number, a dimensionless parameter representing the ratio of inertia force to viscous force in a flow. To realize the objectives of this work, a computational fluid dynamics (CFD) model of fully developed turbulent flow in a pipe is implemented with the help of ANSYS FLUENT 6.3.26 software using two turbulence models namely: The $k-\varepsilon$ and $k-\omega$ models. Fluent software was used to plot the characteristics of the flow and gambit software was used to design the 2D model. In this section, the principles of the CFD with its components are presented.

4.1 Overview of Computational Fluid Dynamics (CFD)

CFD uses numerical methods and algorithms to solve and analyze problems that involve flows by using computers, Tannel *et al* (1997). The working principle of CFD is based on three elements; the pre-processor, solver and post processor.

Pre-processor: Pre-processor consists of the input of the flow problem to a CFD program by means of an operator friendly interface and the subsequent transformation of this input into a form suitable for use by the solver. The region

of fluid to be analyzed is called the computational domain and it is made up a number of discrete elements called the mesh (or grid)

Solver: Solver calculates the solution of the CFD problem by solving the governing equations. The equations governing the fluid motion are Partial Differential Equations (P.D.E) made up of combinations of flow variables (e.g. Velocity and pressure) and derivatives of these variables. Computers cannot directly produce a solution of it. Hence the P.D.E's must be transformed into algebraic equations, Wilcox (2004). This process is known as numerical discretization. There are four methods for it; (i). Finite difference (ii) Finite element method (iii). Finite volume method and (iv).Spectral method. The finite difference and finite volume method both produce solutions to the numerical equations at a given point based on the values of the neighboring points, whereas the finite element produces equations for each element independently of all other elements. In the current work ANSYS FLUENT 6.3.26 which is based on finite volume method is used for the simulation.

Post-processor: It is used to visualize and quantitatively process the results from the solver part. In a CFD package, the analyzed flow phenomena can be presented in vector plots or contour plots to display the trends of velocity, pressure, kinetic energy and other properties of the flow.

The following figure shows the schematic view of the CFD:

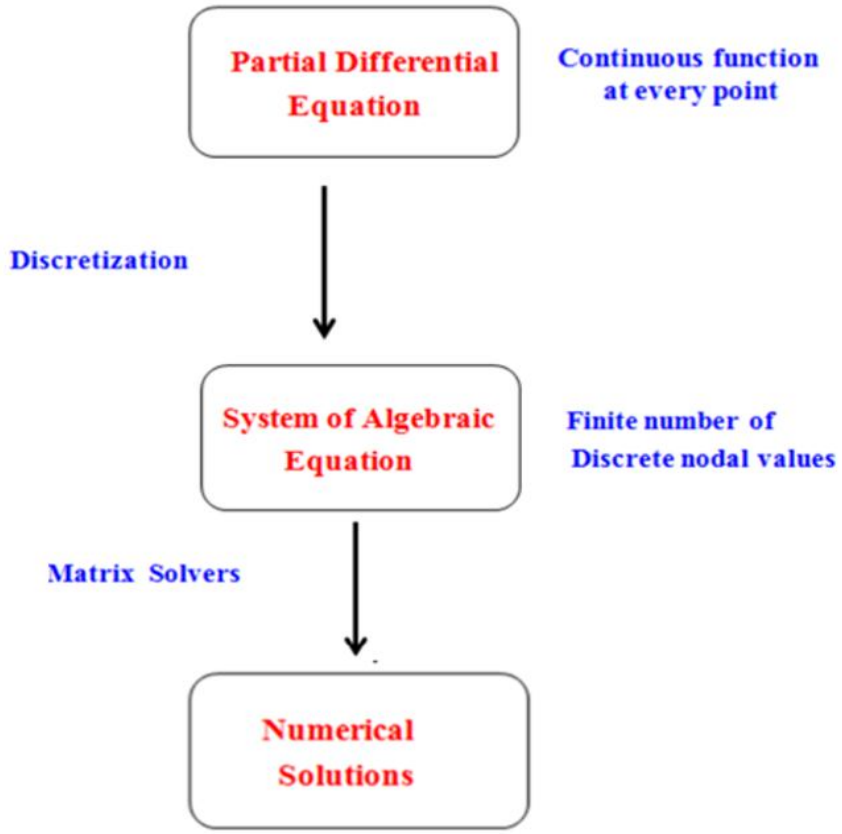

Figure 4.1: Overview of the CFD

4.1.1 Pre-analysis

A turbulent flow exhibits small-scale fluctuations in time. It is usually not possible to resolve these fluctuations in a CFD calculation. So the flow variables such as velocity, pressure, etc. are time-averaged. Unfortunately, the time-averaged governing equations are not closed. (that is, they contain fluctuating quantities which need to be modeled using a turbulence model.) No turbulence model is currently available that is valid for all types of flows and so it is necessary to choose and fine-tune a model for particular classes of flows.

The k-ε and $k-\omega$ models consist of two differential equations: one each for the turbulent kinetic energy k, turbulent dissipation ε and specific dissipation ω. These two equations have to be solved along with the time-averaged continuity, momentum and energy equations.

4.1.2 Reynolds number

This is denoted by *Re* and is defined as the ratio of inertial to viscous forces. Flow in a circular cylinder varies with the Reynolds number. Small Reynolds number corresponds to slow viscous flow where frictional forces are dominant. When Reynolds number increases, flows are characterized by rapid regions of velocity variation and the occurrence of vortices and turbulence. Mathematically, Reynolds number of the flow around a circular cylinder is represented by,

$$\mathrm{Re} = \frac{\rho u D}{\mu}$$

where D is the diameter of the cylinder, u is the inlet velocity of the flow, ρ is a density of fluid and μ is the dynamic viscosity of fluid.

Experimental study of the flow in a circular cylinder has identified regions where significant patterns of flow occur as the Reynolds number changes, especially when the flow changes from laminar to turbulent state. Generally, the following regimes have been identified from experiment, Zdravkovich (1997) as:

Stable range	$40 < Re < 150$
Transition range	$150 < Re < 300$

Irregular range $300 < Re < 200000$

Flow becomes very irregular with instabilities beyond Reynolds number of 200,000. Another dominant feature of the flow in a circular cylinder is the three-dimensional nature of the flow.

4.2. Turbulent velocity profile

Except for flows of very viscous fluids in small diameter ducts, internal flows generally are turbulent. As noted in the relation of shear stress distribution in fully developed pipe flow in turbulent flow there is no universal relationship between the stress field and the mean velocity field. Thus for turbulent flows, we are forced to rely on experimental data. The velocity profile for turbulent flow through a smooth pipe may be approximated by the empirical power-law equation

$$\frac{\bar{u}}{U} = \left(1 - \frac{r}{R}\right)^{1/n} \tag{4.1}$$

Where the exponent (n) varies with the Reynolds number. Data from Hinze (1984) suggests that the variation of power-law exponent n with Reynolds number (based on pipe diameter D and centerline velocity U for fully developed flow in smooth pipe is given by

$$n = -1.7 + 1.8 \log Re \tag{4.2}$$

for $Re > 2x10^4$.

Velocity profiles for n=6 and n=10 are shown below. The parabolic profile for fully developed laminar flow is included for comparison. It is clear that the turbulent profile has a much steeper slope near the wall.

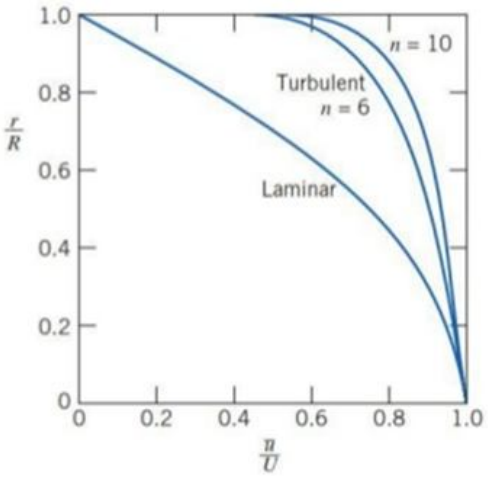

Figure 4.2: velocity profiles for fully developed flow

4.3 Computational details

In the current work, RANS models such as the $k-\varepsilon$ model and the $k-\omega$ model have been chosen to test the suitability and the applicability of the models on the flow in pipes for Reynolds number of 10000. The RANS models used here employ a finite volume method (FVM). The brief details of the simulations are as follows:

4.3.1 Mesh definition

A structured quadrilateral mesh is employed in these simulations. Structured mesh is generated using ANSYS GAMBIT 2.3.16, the grid generation component of ANSYS Fluent 6.3.26, and then imported into ANSYS Fluent. Figure 4.3 displays the

mesh generation in the computational domain. Near to the cylinder wall, very fine mesh is required to resolve boundary layer separation. Quadrilateral cells form the grid structures around the cylinder. To obtain reason-able mesh size for the computational procedure to fully resolve the viscous sub layer, it is necessary to place at least a few cells within $y+ < 5$ and to have $y+ \approx 1$ for the first cell adjacent to the cylinder, ANSYS FLUENT 12.1 Theory Guide (2010). Accordingly, a block-structured mesh type is generated in a rectangular domain.

In order to solve for the flow solution, the geometry is created and meshed in Gambit which is the preprocessor for Fluent. Since the flow is axisymmetric, the geometry is a rectangle. A 100 x 60 mesh (i.e. 100 divisions in the axial direction and 60 divisions in the radial direction) is used to give a fine meshing and increase accuracy.

A smaller grid spacing near the wall is used to resolve the much higher gradient near the wall for a turbulent flow. For each vertical edge, the division length next to the wall is specified as 0.001 and the total number of divisions is 60. Part of the grid is as shown below;

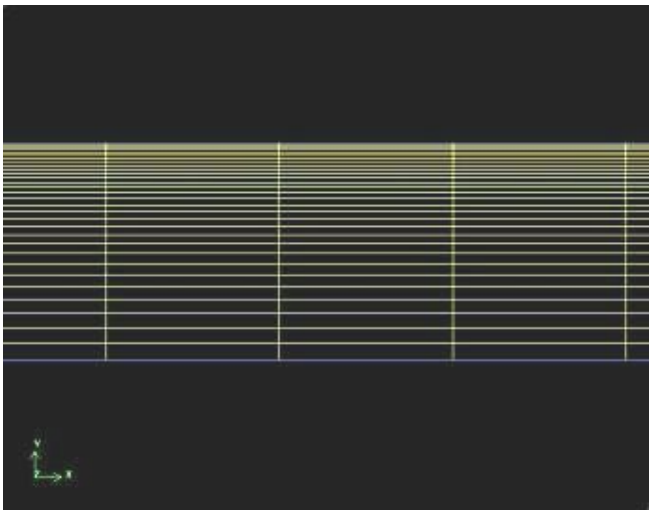

Figure 4.3: Grid along the cylinder

4.4 Boundary conditions

The boundary types for the solution domain shown in figure 4.4 are as follows:

Longitudinal uniform velocities of 1m/s are introduced at the inlet to correspond to Reynolds number of 10,000. In addition, at the inlet the relative turbulent intensity is equal to 5%. The outlet boundary is defined with an average static reference pressure of 0 Pa. A stationary wall (no-slip) boundary condition is prescribed on the top wall of the cylinder, where velocity increases from zero at the wall surface to the free stream velocity away from the surface. On the bottom wall, a symmetry boundary condition is applied. In the model, a wall function approach is used for near- wall treatment. This is specified in GAMBIT as summarized in figure 4.5 below:

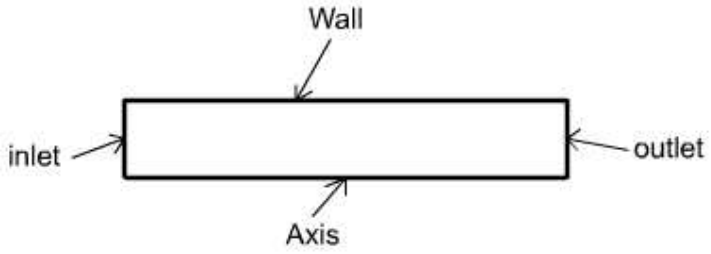

Fig 4.4: Boundary types

4.5 Simulation set-up

The numerical solution of the flow is obtained using ANSYS Fluent 6.3.26. In this 2D-code, discretization is done based on a finite volume approach. In this section the various CFD code settings and options are summarized. A steady and pressure based solver is used. A least square cell based method is used to calculate gradients. Boundary conditions and different discretization schemes are used depending on the turbulence model. They are summarized in Table 1 below. A convergence criteria of 1.0×10^{-6} is set for these simulations.

Table 1: Simulation settings for flow in a pipe with RANS models

Settings	Choice
Simulation type	2D, Steady
Space	Axisymmetric
Solver	Double precision, pressure based, and implicit
Temporal discretization	2^{nd} order
Turbulence model	$k-\varepsilon$ / $k-\omega$ model
Pressure	Standard
Pressure-velocity coupling	SIMPLE
Momentum	2^{nd} order upwind
Turbulent kinetic energy	2^{nd} order upwind
Turbulent dissipation rate (for $k-\varepsilon$ model)	2^{nd} order upwind
Specific dissipation rate (for $k-\omega$ model)	2^{nd} order upwind
Convergence criteria	$1x10^{-6}$
Boundary conditions:	
Inlet	Velocity inlet
Outlet	Pressure outlet
Top wall	No-slip wall
Bottom wall	Axis

4.5.1 Wall Functions

Wall functions are a collection of semi-empirical formulas and functions that in effect bridge "or link" the solution variables at the near-wall cells and the corresponding quantities on the wall. The wall functions comprise:

Laws-of-the-wall for mean velocity and temperature (or other scalars) and formulas for near-wall turbulent quantities. Depending on the choice of turbulent model, ANSYS FLUENT offers three to four choices of wall-function approaches: Standard Wall Functions, Non-Equilibrium Wall Functions, Enhanced Wall Functions (as a part of EWT) and User-Defined Wall Functions.

The standard wall functions in FLUENT are based on the proposal of Launder and Spalding (1974), and have been most widely used for industrial flows. They are provided as a default option in FLUENT.

The law-of-the-wall for mean velocity yields

$$U^+ = \frac{1}{k} In\left(Ey^+\right) \tag{4.3}$$

Where

$$U^+ \equiv \frac{U_P C_\mu^{1/4} k_P^{1/2}}{\tau_w / \rho} \tag{4.4}$$

is the dimensionless velocity

$$y^+ \equiv \frac{\rho C_\mu^{1/4} k_P^{1/2} y_P}{\mu} \tag{4.5}$$

is the dimensionless distance from the wall and

k = von Karman constant (= 0.4187)

E = empirical constant

U_P = mean velocity of the fluid at the near wall node P

k_P = turbulence kinetic energy at the near wall node P

y_P = distance from point P

μ = dynamic viscosity of the fluid

The logarithmic law for mean velocity is known to be valid for 30 < y^+ < 300. In FLUENT, the log-law is employed when y^+ > 11:225.

When the mesh is such that y^+ < 11:225 at the wall-adjacent cells, FLUENT applies the laminar stress-strain relationship that can be written as

$$U^+ = y^+ \tag{4.6}$$

In FLUENT, the laws-of-the-wall for mean velocity and temperature are based on the wall unit, y^+ These quantities are approximately equal in equilibrium turbulent boundary layers.

4.5.2 Enhanced Wall Treatment

Enhanced Wall Treatment is used to get a more accurate result. In FLUENT's near-wall model, the viscosity-affected near-wall region is completely resolved all the way to the viscous sublayer. The two-layer approach is an integral part of the enhanced wall treatment and is used to specify both ε and the turbulent viscosity in the near wall cells. In this approach the whole domain is subdivided into a viscosity- affected region and a fully turbulent region. The demarcation of the two regions is determined by a wall-distance based, turbulent Reynolds number *Re* defined as

$$Re \equiv \frac{\rho y \sqrt{k}}{\mu} \tag{4.7}$$

where y is the normal distance from the wall at cell centers. In FLUENT, y is interpreted as the distance to the nearest wall:

$$y \equiv \min_{\vec{r}_w \in \Gamma_w} \|\vec{r} - \vec{r}_w\| \tag{4.8}$$

where $\vec{r}$ is the position vector at the field point, and $\vec{r}_w$ is the position vector on the wall boundary. Γ_w is the union of all wall boundaries involved. This interpretation allows y to be uniquely defined in flow domains of complex shape involving multiple walls. Furthermore, y defined in this way is independent of the mesh topology used, and is definable even on unstructured meshes. In the fully turbulent region, the $k-\varepsilon$ models or the RSM are employed. In the viscosity-affected near-wall region the one-equation model is employed. The two-layer formulation for turbulent viscosity is used as part of the enhanced wall treatment, in which the two-layer definition is smoothly blended with the high-Reynolds-number μ_t definition from the outer region, as proposed by Jongen (1992)

$$\mu_t = \lambda_\varepsilon \mu_t + (1-\lambda_\varepsilon)\mu_t \tag{4.9}$$

where μ_t is the high-Reynolds-number definition. A blending function, λ_ε, is defined in such a way that it is equal to unity far from walls and is zero very near to walls. The blending function chosen is

$$\lambda_\varepsilon = \frac{1}{2}\left[1 + \tanh\left(\frac{\mathrm{Re}_y - \mathrm{Re}_y^*}{A}\right)\right] \tag{4.10}$$

The constant A determines the width of the blending function. By defining a width such that the value of λ_ε will be within 1% of its far-field value given a variation of $\Delta \mathrm{Re}_y$ the result is

$$A = \frac{\left|\Delta \mathrm{Re}_y\right|}{\tanh(0.98)} \tag{4.11}$$

Typically, $\Delta \mathrm{Re}_y$ would be assigned a value that is between 5% and 20% of Re_y^*. The main purpose of the blending function λ_ε is to prevent solution convergence from being impeded when the $k-\varepsilon$ solution in the outer layer does not match with the two-layer formulation.

The ε field is computed from

$$\varepsilon = \frac{k^{3/2}}{\ell_\varepsilon} \tag{4.12}$$

The length scales that appear in Equation (4.12) are computed from Chen and Patel (1988) that is:

$$\ell_\varepsilon = yc_\ell\left(1 - e^{-\mathrm{Re}_y/A_\varepsilon}\right) \tag{4.13}$$

If the whole flow domain is inside the viscosity-affected region (Rey < 200), ε is not obtained by solving the transport equation; it is instead obtained algebraically from Equation 4.12, FLUENT uses a procedure for the ε specification that is similar to the turbulent viscosity blending in order to ensure a smooth transition between the algebraically-specified ε in the inner region and the ε obtained from solution of the transport equation in the outer region.

The constants in the length scale formulas, Equation (4.13) are taken from Chen and Patel (1988):

$$c_\ell = kC_\mu^{3/4}\ , A_\varepsilon = 2c_\ell \tag{4.14}$$

4.5.3 Standard Wall Functions

To have a method that can extend its applicability throughout the near-wall region (i.e., laminar sublayer, buffer region, and fully-turbulent outer region) it is necessary to formulate the law-of-the wall as a single wall law for the entire wall region. FLUENT achieves this by blending linear (laminar) and logarithmic (turbulent) laws-of-the-wall using a function suggested by Kader (1981):

$$u^+ = e^{\Gamma} u_{lam}^+ + e^{\frac{1}{\Gamma}} u_{turb}^+ \tag{4.15}$$

where the blending function is given by:

$$\Gamma = -\frac{a\left(y^+\right)^4}{1+by^+} \tag{4.16}$$

where a = 0:01 and b = 5.

Similarly, the general equation for the derivative $\frac{du^+}{dy^+}$ is

$$\frac{du^+}{dy^+} = e^{\Gamma}\frac{du_{lam}^+}{dy^+} + e^{\frac{1}{\Gamma}}\frac{du_{turb}^+}{dy^+} \tag{4.17}$$

This approach allows the fully turbulent law to be easily modified and extended to take into account other effects such as pressure gradients or variable properties. This formula also guarantees the correct asymptotic behavior for large and small values of y+ and reasonable representation of velocity profiles in the cases where y+ falls inside the wall buffer region ($3 < y^+ < 10$).

The enhanced wall functions were developed by smoothly blending an enhanced turbulent wall law with the laminar wall law. The enhanced turbulent law-of-the-wall for compressible flow with heat transfer and pressure gradients has been derived by combining the approaches of White and Cristoph (1971) and Huang *et al* (1993):

$$\frac{du^+_{turb}}{dy^+} = \frac{1}{ky^+}\left[S'\left(1-\beta u^+ - \gamma\left(u^+\right)^2\right)\right]^{\frac{1}{2}} \tag{4.18}$$

where

$$S' = \begin{cases} 1+\alpha y^+ & for\ y^+ < y_s^+ \\ 1+\alpha y_s^+ & for\ y^+ \geq y_s^+ \end{cases} \tag{4.19}$$

and

$$\alpha \equiv \frac{v_w}{\tau_w u^*}\frac{dp}{dx} = \frac{\mu}{\rho^2\left(u^*\right)^3}\frac{dp}{dx} \tag{4.20}$$

$$\beta \equiv \frac{\sigma_t q_w u^*}{c_p \tau_w T_w} = \frac{\sigma_t q_w}{\rho c_p u^* T_w} \tag{4.21}$$

$$\gamma \equiv \frac{\sigma_t\left(u^*\right)^2}{2c_p T_w} \tag{4.22}$$

where y_s^+ is the location at which the log-law slope will remain fixed. By default, y_s^+ = 60. The coefficient α in Equation (4.20) represents the influences of pressure gradients while the coefficients β and γ represent thermal effects. Equation (4.19) is an ordinary differential equation and FLUENT will provide an appropriate analytical solution. If α, β and γ all equal 0, an analytical solution would lead to the classical turbulent logarithmic law-of-the-wall.

The boundary condition for turbulence kinetic energy is the same as for standard wall functions. However, the production of turbulence kinetic energy G_k is computed using the velocity gradients that are consistent with the enhanced law-of-the wall ensuring a formulation that is valid throughout the near-wall region.

4.5.4 Turbulence

In the $k-\varepsilon$ models and in the RSM (if the option to obtain wall boundary conditions from the *k* equation is enabled), the *k* equation is solved in the whole domain including the wall-adjacent cells. The boundary condition for *k* imposed at the wall is

$$\frac{\partial k}{\partial n} = 0 \tag{4.23}$$

where n is the local coordinate normal to the wall.

The production of kinetic energy G_k and its dissipation rate ε at the wall-adjacent cells, which are the source terms in the *k* equation, are computed on the basis of the local equilibrium hypothesis. Under this assumption, the production of *k* and its dissipation rate are assumed to be equal in the wall-adjacent control volume.

Thus, the production of *k* is computed from, ANSYS FLUENT 12.1 Theory Guide, (2010):

$$G_k \approx \tau_w \frac{\partial U}{\partial y} = \tau_w \frac{\tau_w}{k\rho C_\mu^{1/4} k_p^{1/2} y_p} \tag{4.24}$$

and ε is computed from

$$\varepsilon_p = \frac{C_\mu^{3/4} k_p^{3/2}}{k y_p} \tag{4.25}$$

The ε equation is not solved at the wall-adjacent cells, but instead is computed using equation (4.25). The wall boundary conditions for the solution variables, including mean velocity, temperature, k, and ε, are all taken care of by the wall functions. The standard wall functions described so far are provided as a default option in FLUENT. The standard wall functions work reasonably well for a broad range of wall-bounded flows. However, they tend to become less reliable when the flow situations depart too much from the ideal conditions that are assumed in their derivation. Among others, the constant shear and local equilibrium hypotheses are the ones that most restrict the universality of the standard wall functions. Accordingly, when the near-wall flows are subjected to severe pressure gradients, and when the flows are in strong non-equilibrium, the quality of the predictions is likely to be compromised.

4.5.5 Discretization

FLUENT uses a control-volume-based technique to convert the governing equations to algebraic equations that can be solved numerically. This control volume technique consists of integrating the governing equations about each control volume, yielding discrete equations that conserve each quantity on a control-volume basis. Discretization of the governing equations can be illustrated most easily by considering the steady-state conservation equation for transport of a scalar quantity ϕ. This is demonstrated by the following equation written in integral form for an arbitrary control volume V as follows:

$$\oint \rho\phi \vec{v} \cdot d\vec{A} = \oint \Gamma_\phi \nabla\phi \cdot d\vec{A} + \int_V S_\phi dV \tag{4.26}$$

where

$\rho =$ density

$\vec{v} =$ velocity vector $\left(= u\hat{i} + v\hat{j}\ in\ 2D\ \right)$

$\vec{A} =$ surface area vector

$\Gamma_\phi =$ diffusion coefficient for ϕ

$\nabla\phi =$ gradient of ϕ $\left(= {}^{\partial\phi}\!/_{\partial x}\hat{i} + {}^{\partial\phi}\!/_{\partial y}\hat{j}\ in\ 2D\right)$

$S_\phi =$ source of ϕ per unit volume

Equation (4.26) is applied to each control volume, or cell, in the computational domain. The two-dimensional, triangular cell shown in Figure 4.6 is an example of such a control volume. Discretization of equation (4.26) on a given cell yields

$$\sum_f^{N_{faces}} \rho f\, \vec{v}_f\, \phi_f \cdot \vec{A}_f = \sum_f^{N_{faces}} \Gamma_\phi (\nabla\phi)_n \cdot \vec{A}_f + S_\phi V \tag{4.27}$$

where

N_{faces} = number of faces enclosing cell

ϕ_f = value of ϕ convected through face f

$\rho f\, \vec{v}_f\, \phi_f \cdot \vec{A}_f$ = mass flux through the face

$\vec{A}_f$ = area of face f, $|A|\left(= \left|A_x\hat{i} + A_y\hat{j}\right| in\ 2D\right)$

$(\nabla\phi)_n$ = magnitude of $\nabla\phi$ normal to face f

V = cell volume

The equations solved by FLUENT take the same general form as the one given above (4.27) and apply readily to multi-dimensional, unstructured meshes composed of arbitrary polyhedra. By default, FLUENT stores discrete values of the scalar ϕ at the cell centers (c0 and c1 in Figure 4.6). However, face values ϕ_f are required for the convection terms in Equation (4.27) and must be interpolated from the cell center values. This is accomplished using an upwind scheme. Upwinding means that the face value ϕ_f is derived from quantities in the cell upstream, or "upwind," relative to the direction of the normal velocity v_n in equation (4.27). The diffusion terms in equation (4.27) are central-differenced and are always second order accurate.

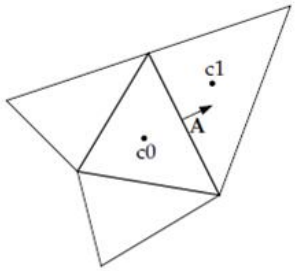

Figure 4.5: Control Volume used to illustrate Discretization

4.5.6 Second-Order Upwind Scheme

When second-order accuracy is desired, quantities at cell faces are computed using a multidimensional linear reconstruction approach Barth and Jespersen (1989). In this approach, higher-order accuracy is achieved at cell faces through a Taylor series expansion of the cell-centered solution about the cell centroid. Thus when

second-order upwinding is selected, the face value ϕ_f is computed using the following expression:

$$\phi_f = \phi + \nabla\phi \cdot \Delta\vec{s}$$

where ϕ and $\nabla\phi$ are the cell-centered value and its gradient in the upstream cell, and $\Delta\vec{s}$ is the displacement vector from the upstream cell centroid to the face centroid. This formulation requires the determination of the gradient $\nabla\phi$ in each cell. This gradient is computed using the divergence theorem, which in discrete form is written as

$$\nabla\phi = \frac{1}{V}\sum_{f}^{N_{\text{faces}}} \tilde{\phi}_f \vec{A} \tag{4.28}$$

Here the face values $\tilde{\phi}_f$ are computed by averaging ϕ from the two cells adjacent to the face. Finally, the gradient $\nabla\phi$ is limited so that no new maxima or minima are introduced.

4.5.7 Pressure-Velocity Coupling

The SIMPLE (Semi-Implicit Method for Pressure-Linked Equations) family of algorithms. Patankar (1980) is used for introducing pressure into the continuity equation. Pressure-velocity coupling is achieved by deriving an equation for pressure from the discrete continuity equation. The coupled solver in FLUENT solves the governing equations of continuity, momentum and (where appropriate) energy and species transport simultaneously as a set, or vector of equations.

The system of governing equations for a single-component fluid, written to describe the mean flow properties, is cast in integral, Cartesian form for an arbitrary control volume V with differential surface area d**A** as follows:

$$\frac{\partial}{\partial t}\int_V \mathbf{W}\,dV + \oint [\mathbf{F}-\mathbf{G}]\cdot d\mathbf{A} = \int_V \mathbf{H}\,dV \tag{4.29}$$

where the vectors **W, F** and **G** are defined as:

$$\mathbf{W} = \begin{Bmatrix} \rho \\ \rho u \\ \rho v \\ \rho w \\ \rho E \end{Bmatrix}, \quad \mathbf{F} = \begin{Bmatrix} \rho \mathbf{v} \\ \rho \mathbf{v} u + p\hat{\mathbf{i}} \\ \rho \mathbf{v} v + p\hat{\mathbf{j}} \\ \rho \mathbf{v} w + p\hat{\mathbf{k}} \\ \rho \mathbf{v} E + p\mathbf{v} \end{Bmatrix}, \quad \mathbf{G} = \begin{Bmatrix} 0 \\ \tau_{xi} \\ \tau_{yi} \\ \tau_{zi} \\ \tau_{ij} v_j + \mathbf{q} \end{Bmatrix} \tag{4.30}$$

and the vector **H** contains source terms such as body forces and energy sources. Here ρ, **v**, E, and p are the density, velocity, total energy per unit mass, and pressure of the fluid, respectively. τ is the viscous stress tensor, and **q** is the heat flux.

For all flows, FLUENT uses the gauge pressure internally. Any time an absolute pressure is needed, it is generated by adding the operating pressure (101,325 Pa) to the gauge pressure. The (absolute) pressure at the outlet is 1 atm. Since the operating pressure is set to 1 atm, the outlet gauge pressure = outlet absolute pressure - operating pressure = 0.

4.5.8 Convergence

Starting with excessively crude initial guesses for mean and turbulence quantities may cause the solution to diverge. A safe approach is to start your calculation

using conservative (small) under-relaxation parameters and (for the coupled solvers) a conservative Courant number, and increase them gradually as the iterations proceed and the solution begins to settle down.

For faster convergence you start with reasonable initial guesses for the *k* and ε (or *k* and ω) fields. Particularly when the enhanced wall treatment is used, it is important to start with a sufficiently developed turbulence field in order to avoid the need for an excessive number of iterations to develop the turbulence field. The convergence criteria has been set for the *k* and ε equations and *k* and ω in addition to the equations of continuity and momentum.

FLUENT reports a residual for each governing equation being solved. The residual is a measure of how well the current solution satisfies the discrete form of each governing equation. We'll iterate the solution until the residual for each equation falls below 1x 10^{-6}.

4.5.9 Providing an Initial Guess for k- ε and k-ω

For flows using one of the $k-\varepsilon$ models, or one of the $k-\omega$ models, the converged solutions or (for unsteady calculations) the solutions after a sufficiently long time has elapsed should be independent of the initial values for *k* and ε (or *k* and ω). For better convergence, however, it is beneficial to use a reasonable initial guess for *k* and ε (or *k* and ω).The initial guess is constant over the flow domain and equal to the values at the inlet: axial velocity (1m/s), radial velocity (0 m/s), gauge pressure (0 pa). The Turbulent Kinetic Energy and Dissipation rate/Specific

Dissipation rate are set from prescribed values for the Turbulent intensity (5%) and hydraulic/pipe diameter at the inlet.

In general, it is recommended to start from a fully-developed state of turbulence. When using the enhanced wall treatment for the $k-\varepsilon$ model it is important to specify fully-developed turbulence fields. Specifying reasonable boundary conditions at the inlet, helps in the computation of the initial values for k and ε (or k and ω) in the whole domain from these boundary values.

Analysis of fluid flow using RANS $k-\varepsilon$ and $k-\omega$ models at a constant Reynolds number of 10,000 is presented in the next chapter. A comparison of results obtained from the CFD simulation are presented and discussed.

CHAPTER FIVE

RESULTS AND DISCUSSION

5.0 Overview

In this chapter, the results of the simulations are presented followed by a discussion at each step. The simulations are carried out for Reynolds number of 10,000.The solutions of the model are obtained by first converting the Partial Differential Equations into algebraic equations. FLUENT is then used to output the required profiles. The various parameters such as centerline velocity, skin friction coefficient, outlet velocity profile and turbulent intensity and have been investigated with each turbulence model for various pipe diameters (D). In the present study the simulations are compared against experimental results of Bhandari and Singh (2012). Besides these previous works, a number of formulations and analytical results have been discussed in various books. The expression defining the velocity distribution in a pipe flow across turbulent flow is derived and demonstrated in Bejan (1994). The relationships defining friction in pipes have been demonstrated in White (1994).

In this section results with D = 0.25m, D = 1m, D=5m and D = 10m respectively are presented. For this purpose two different models: the $k-\varepsilon$ and the $k-\omega$ model are used.

5.1 Grid

Here all simulations have been done using a grid which contains 6000 quadrilateral cells. The detailed information is given below:

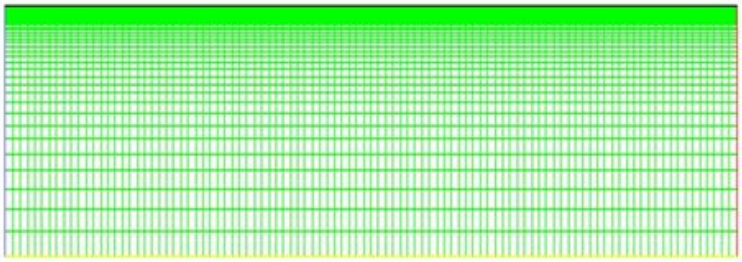

Figure 5.1: Grid size

```
Grid Size

Level    Cells    Faces    Nodes   Partitions
    0     6000    12160     6161            1

 1 cell zone, 5 face zones.
```

5.2 Residuals:

The residual is a measure of how well the current solution satisfies the discrete form of each governing equation being solved. We iterate the solution until the residual for each equation falls below 1×10^{-6}.

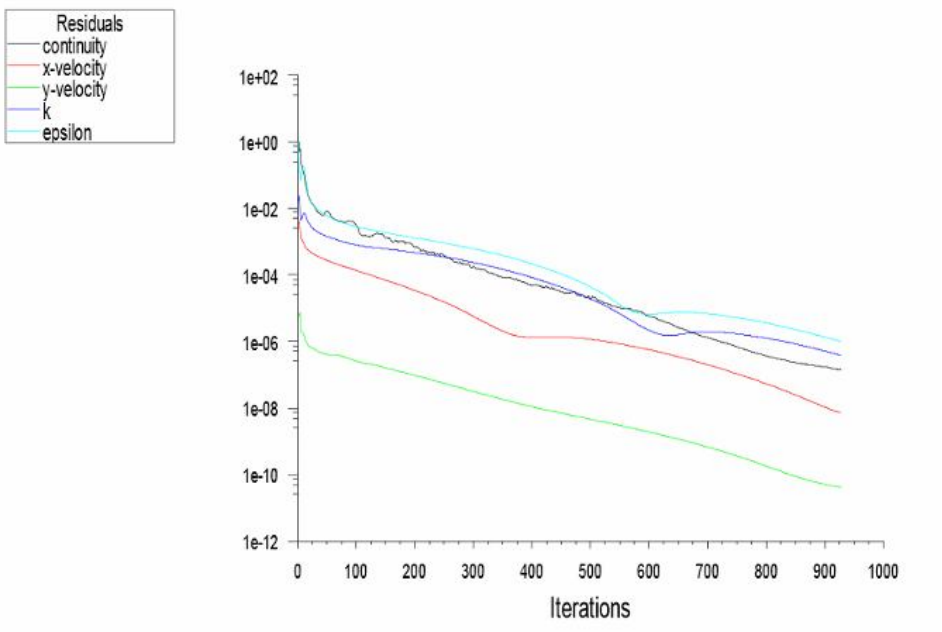
Residuals
continuity
x-velocity
y-velocity
k
epsilon
1e+02
1e+00
1e-02
1e-04
1e-06
1e-08
1e-10
1e-12
0
100
200
300
400
500
600
700
800
900
1000
Iterations

(i)

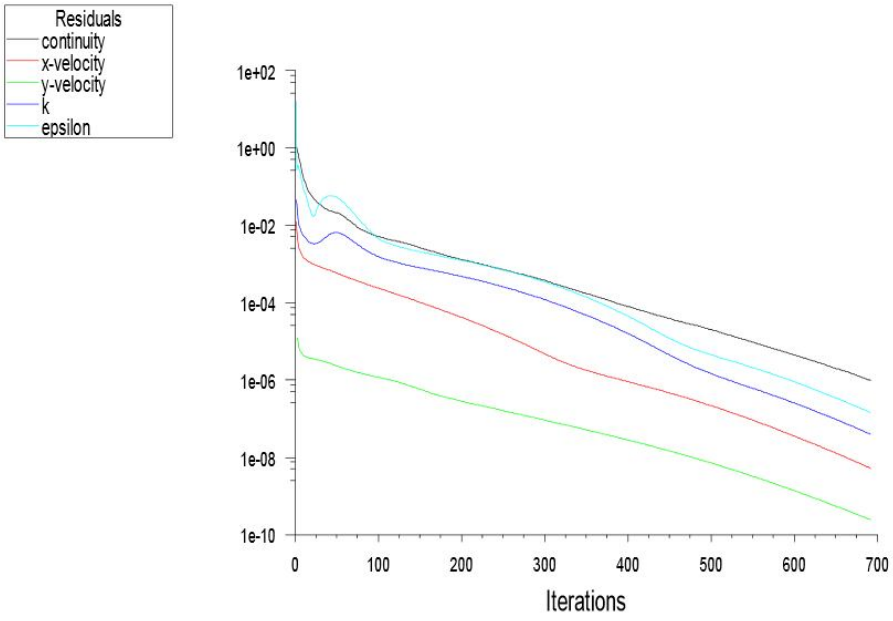
Residuals
continuity
x-velocity
y-velocity
k
epsilon
1e+02
1e+00
1e-02
1e-04
1e-06
1e-08
1e-10
0
100
200
300
400
500
600
700
Iterations

(ii)

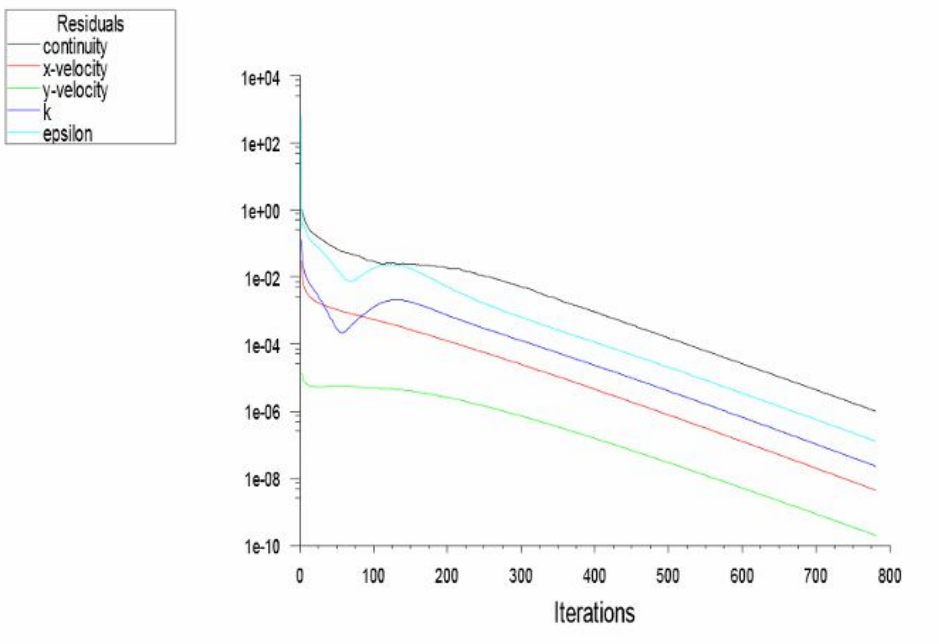

(iii)

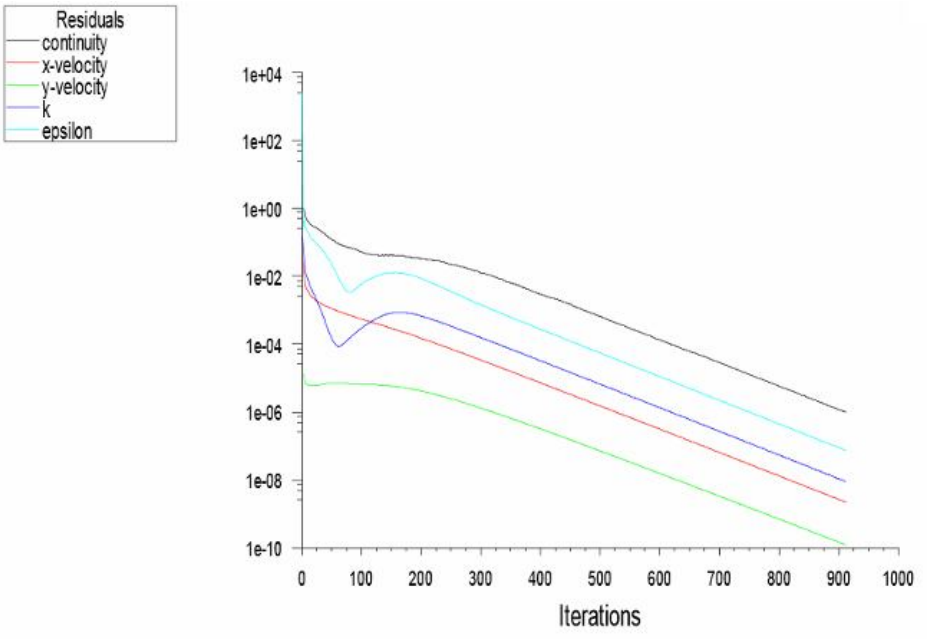

(iv)

Figure 5.2 (a): Residuals: (i) D = 0.25m (ii) D = 1m (iii) D = 5m and (iv) D = 10m for $k-\varepsilon$ model

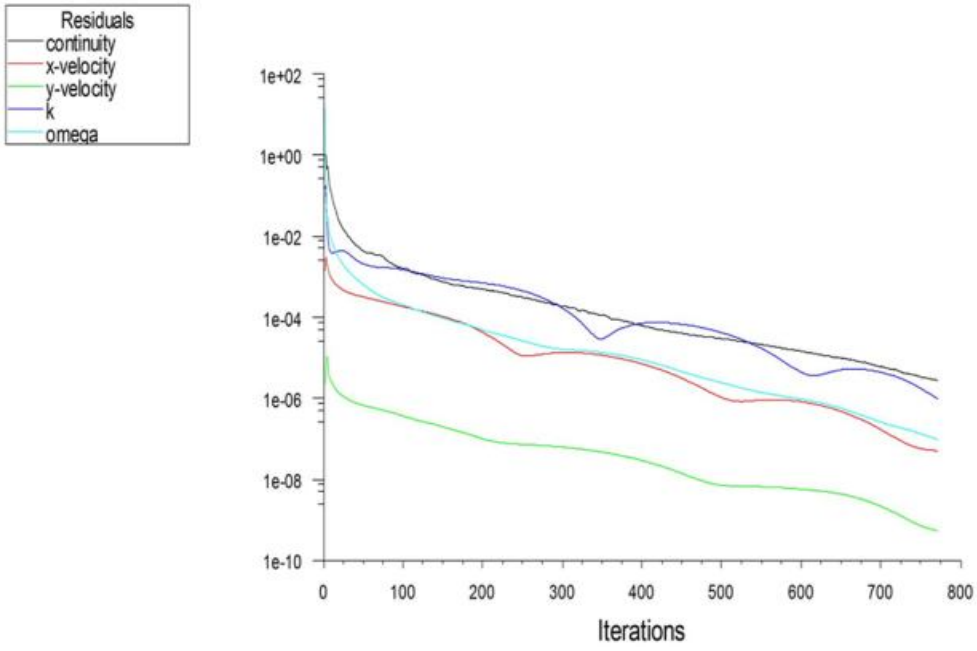
Residuals
continuity
x-velocity
y-velocity
k
omega
1e+02
1e+00
1e-02
1e-04
1e-06
1e-08
1e-10
0
100
200
300
400
500
600
700
800
Iterations

(i)

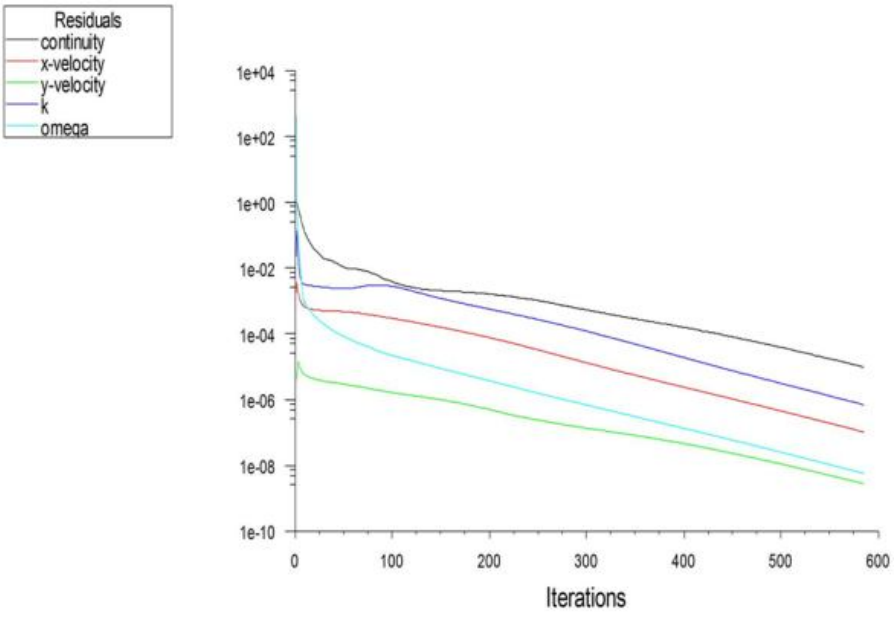
Residuals
continuity
x-velocity
y-velocity
k
omega
1e+04
1e+02
1e+00
1e-02
1e-04
1e-06
1e-08
1e-10
0
100
200
300
400
500
600
Iterations

(ii)

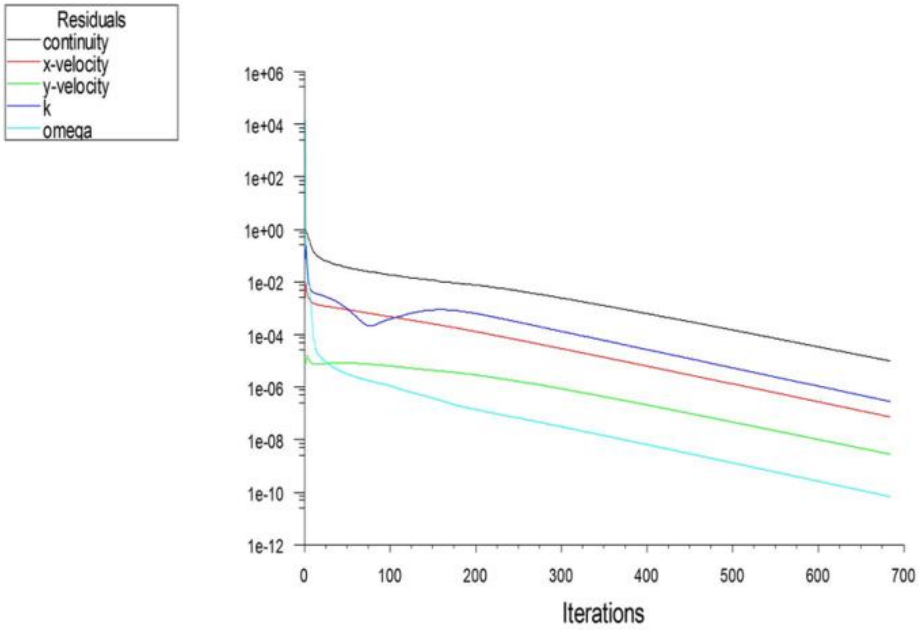

(iii)

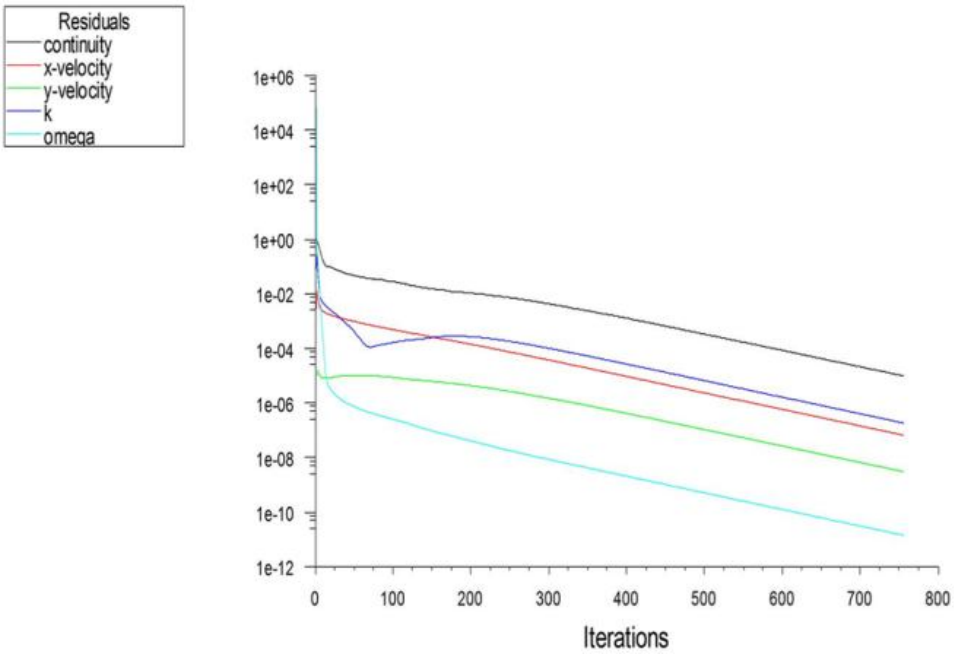

(iv)

Figure 5.2 (b): Residuals (i) D = 0.25m (ii) D= 1m (c) D=5m (iv) D = 10m for $k-\omega$ model

The residuals fall below the specified convergence criterion of 1 x 10^{-6} after a number of iterations. Actual number of convergence steps varies slightly in the two models for the corresponding diameters. In the $k-\varepsilon$ model, pipe with diameter 0.25m converges after 927 iterations, diameter 1m after 691 iterations, diameter 5m after 781 iterations and diameter 10m after 912 iterations. Using the $k-\omega$ model they converge after 771, 585, 684 and 756 iterations respectively.

The number of iterations for the two models shows a similar pattern, but the $k-\omega$ model converges faster for all the pipes. The small difference between the number of iterations in the two models is due to the different value of their diffusion model constant. The $k-\omega$ model enjoys advantages over the $k-\varepsilon$ model, especially for integrating through the viscous sub layer and for predicting effects of adverse pressure gradient.

5.3 Plotting *y+* values for wall-adjacent cells

The wall y^+ is a non-dimensional number similar to local Reynolds number, determining whether the influences in the wall-adjacent cells are laminar or turbulent, hence indicating the part of the turbulent boundary layer that they resolve. Figure 5.3 shows the results obtained from the two models.

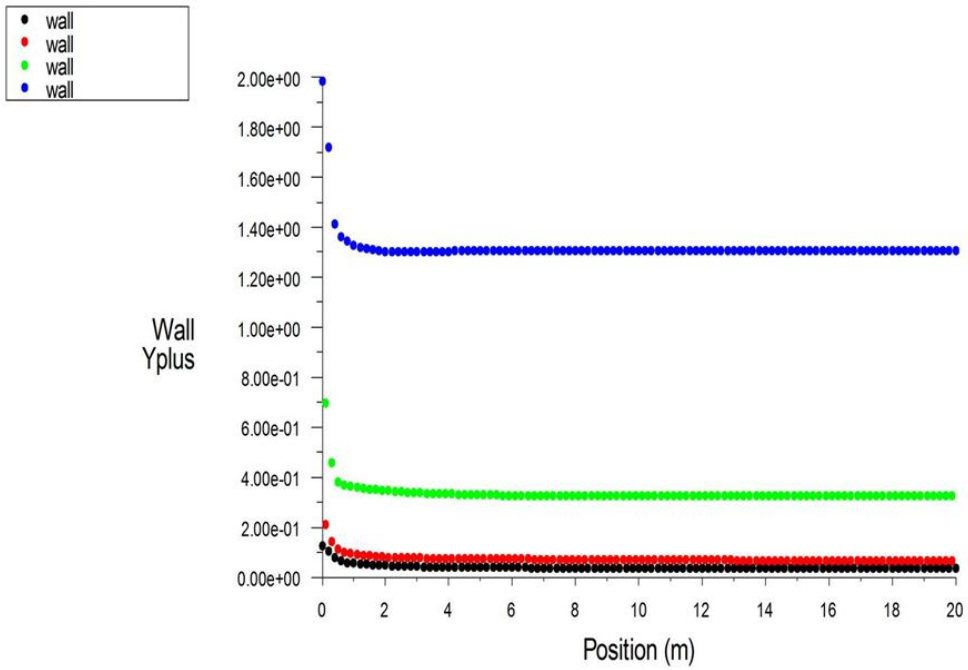

Figure 5.3 (a): Wall y^+: (i) D = 0.25m (blue) (ii) D = 1m (green) (iii) D = 5m (red) and (iv) D = 10m (black) for $k-\varepsilon$ model

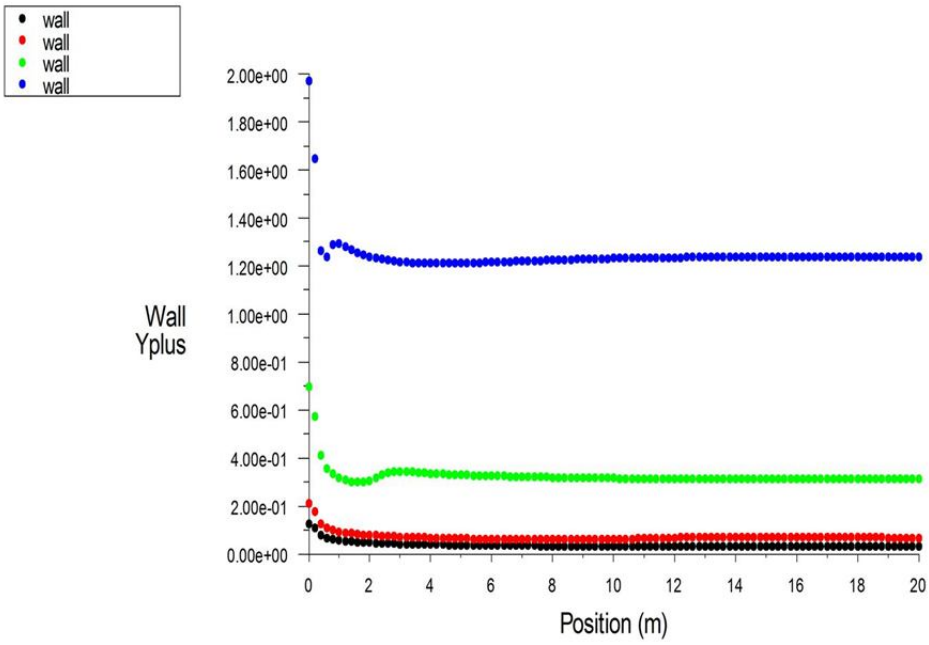

Figure 5.3 (b): Wall y^+: (i) D = 0.25m (blue) (ii) D = 1m (green) (iii) D = 5m (red) and (iv) D = 10m (black) for $k-\omega$ model

There is a sharp drop in the y^+ values for all the three pipes at the inlet. In Fig 5.3 (a), the y^+ value of Pipe with diameter 0.25m drops from 2.00 to 1.30 a distance of 2m from the inlet after which it remains constant up to the outlet. Pipe with diameter 1m has a y^+ value which drops from 0.7 to 0.35 at the inlet. The y^+ values for pipe with diameter 5m and 10m drops slightly from 0.2 and 0.1 to 0.05 where it is maintained up to the outlet.

In Fig.5.3 (b), (i), the y^+ value of Pipe with diameter 0.25m drops sharply from 2.0 to 1.2 a distance of 0.5m from the inlet after which it increases slightly and drops again to 1.2 up to the outlet. Pipe with diameter 1m has a y^+ value which drops sharply from 0.7 at the inlet to 0.3 .A slight increase follows 2m away from the inlet up to 0.35 where it remains steady throughout the pipe. The y^+ values for pipe with diameter 5m and 10m drops slightly from 0.22 and 0.12 respectively at inlet then it is maintained at 0.05 and 0.07 respectively up to the outlet.

For all cases the y^+ is seen to be less than 5, therefore the near-wall grid resolution is acceptable. This means that we can resolve the turbulent eddies down into the viscous sub layer. For all the four pipes it can be observed that there are no changes in these profiles with time, that is away from the inlet. A larger initial y^+ value is as a result of the role played by distortions of the inlet velocity profile and finite amplitude disturbances due to entry effects. Scalable wall functions activate the usage of the log law in regions where the y^+ is sufficiently small in conjunction with the standard wall function approach in coarser y^+ regions. A smaller overall

mesh count in pipes with smaller diameters leads to faster run times and this explains the slightly higher y^+ values. The cross-stream width of the region over which changes take place is small compared to any length scale in the flow direction.

The $k-\varepsilon$ turbulence model is primarily valid away from walls and special treatment is required to make it valid near walls. The near-wall model is sensitive to the grid resolution which is assessed in the wall unit y^+. A very fine mesh is require near the wall to resolve the turbulent eddies in the boundary layer. To use a wall function approach for a particular turbulence model, we need to ensure that our y^+ values are within a certain range. For Fluent we select the near-wall resolution such that $y^+ > 30$ or < 5 for the wall-adjacent cell.

5.4 Axial velocity

Developing length can be determined through the XY plot for centerline velocity. The distance from the pipe inlet to the stream wise location where centerline velocity does not change anymore is the developing or entry length. Figures 5.4(a) and (b) shows graphs of the axial velocity as a function of the distance along the centerline of the pipe.

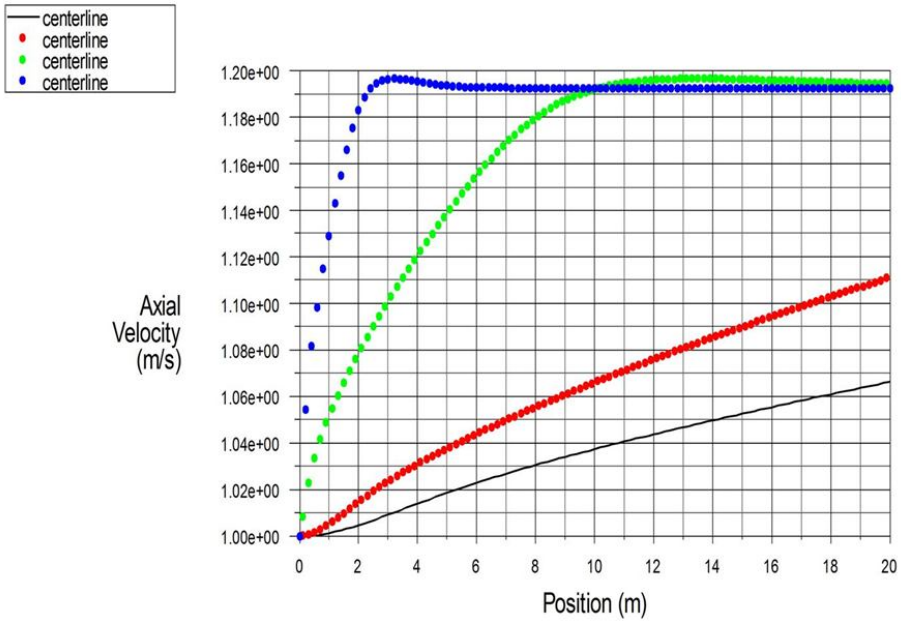

Figure 5.4 (a): Axial velocity (i) D = 0.25m (blue) (ii) D = 1m (green) (iii) D = 5m (red) and (iv) D = 10m (black) for $k-\varepsilon$ model

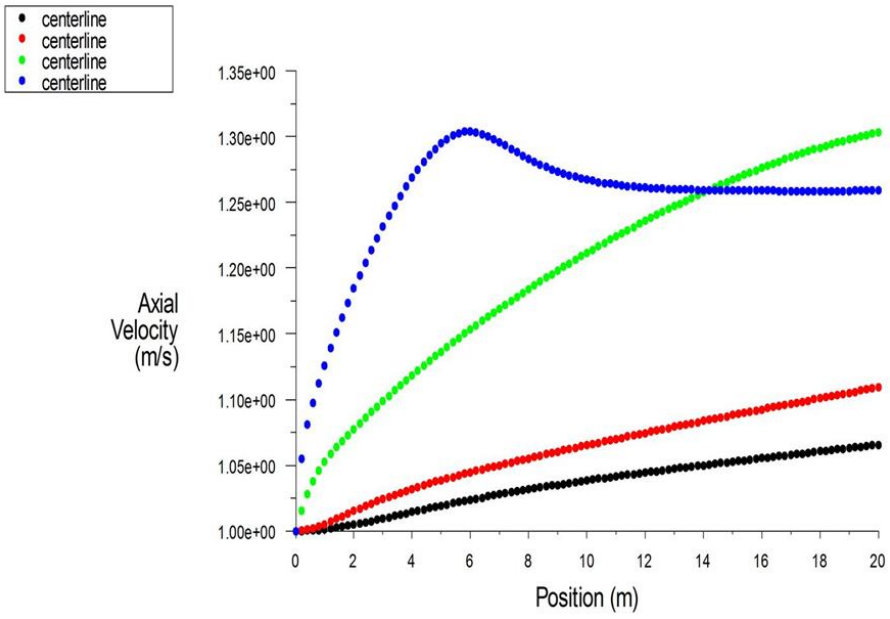

Figure 5.4 (b): Axial velocity (i) D = 0.25m (blue) (ii) D = 1m (green) (iii) D = 5m (red) and (iv) D = 10m (black) for $k-\omega$ model

In fig 5.4 (a), (i) and (ii), the velocity reaches a constant value beyond a certain distance from the inlet: x = 6m and x = 11m respectively. This is the fully-developed flow region where the centerline velocity becomes a constant. Fig (iii) and (iv) shows the velocity increasing steadily from 1m/s to 1.11m/s and 1.09m/s respectively at the outlet.

In fig. 5.4 (b) (i), for the first 6m from the inlet, there is an increase in velocity from 1m/s to 1.3m/s then it decreases gradually to 1.25m/s and remains constant throughout the pipe. Fig. 5.4 (b) (ii) shows an increase in velocity from 1m/s to 1.30m/s at the outlet. In figure (iii) and (iv) the velocity increases linearly but gradually from 1m/s at the inlet to 1.12m/s and 1.08 respectively at the outlet.

From figures 5.4 (a) and (b), it can be observed that the flow rate decreases when the diameter is increased. This is as a result of an increase in turbulent intensity. Predictions by the two models is good and follows the trend of the experimental data by Bhandari and Singh (2012).

Flow towards center of the pipe tends to flow faster in the flow direction. When a fluid enters a circular pipe at a uniform velocity, because of the no-slip condition, the fluid particles in the layer in contact with the surface of the pipe come to a complete stop. This layer also causes the fluid particles in the adjacent layers to slow down gradually as a result of friction. To make up for this velocity reduction, the velocity of the fluid at the midsection of the pipe has to increase to keep the mass flow rate through the pipe constant.

As a result a velocity gradient develops along the pipe. The $k-\varepsilon$ model gives excellent agreement with experimental results for the centerline velocity. The centerline velocity for fully developed region is around 1.19m/s while the value calculated analytically is 1.22 m/s. The $k-\omega$ model is insensitive to grid resolution and over predicts the velocity at the centerline.

As the flow develops downstream of the inlet, the viscous boundary layer grows, and will eventually fill the pipe completely (provided that the tube is long enough). When this happens, the flow becomes fully developed and there is no variation of the velocity profile in the axial direction. The entrance effects become insignificant beyond a pipe length of 10 diameters and this is called the hydrodynamic entry length approximated as 10D, where D is the pipe diameter. That is the reason why the pipes with diameters 5m and 10m have not attained a constant value downstream, their length are not long enough. The boundary layer builds up much faster in smaller diameters and this explains why the pipes with smaller diameters reach a constant velocity after a shorter distance from the inlet. The $k-\varepsilon$ model however shows good predictions of the onset of the entry length as demonstrated in Bejan (1994).

The vector plots for the velocity magnitudes are as shown below:

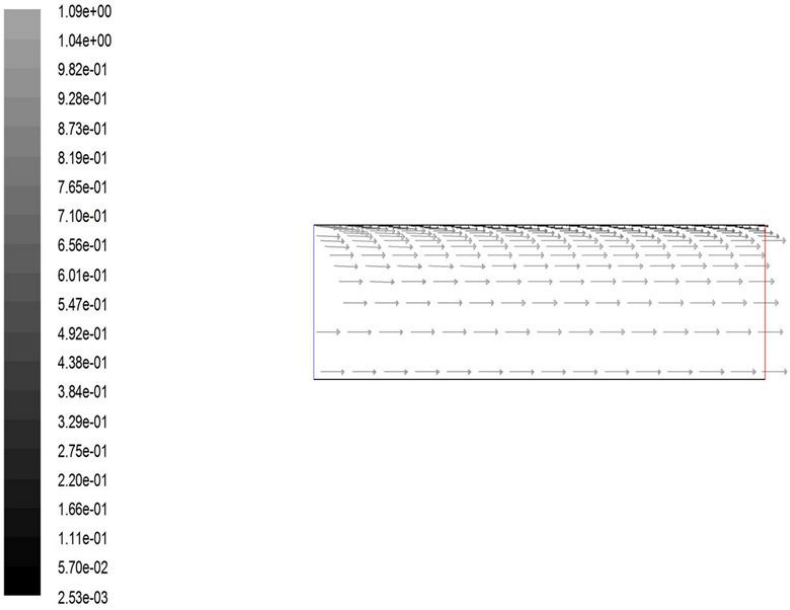

Figure 5.4 (c): Vector plots for velocity magnitudes for $k-\varepsilon$ and $k-\omega$

The vector magnitudes are minimum at the wall and increase towards the centerline This is indicated by the size of the arrows and is true for all pipe diameters and both models and is in agreement with no-slip condition along the wall and higher velocities at the centerline for conservation of mass.

5.5 Skin Friction Coefficient

Skin Friction Coefficient, C_f , is a non-dimensional parameter defined as the ratio of the wall shear stress and the reference dynamic pressure (i.e. pressure resulting from the conversion of Kinetic Energy of the flow into pressure). It is expressed as:

$$C_f \equiv \frac{\tau_w}{\frac{1}{2}\rho v^2} \tag{5.1}$$

where τ_w is the wall shear stress, and ρ and v are the fluid density and velocity at the inlet respectively. The dynamic pressure is defined by $\frac{1}{2}\rho v^2$.

Plotting the friction coefficient along the top wall gives the following results:

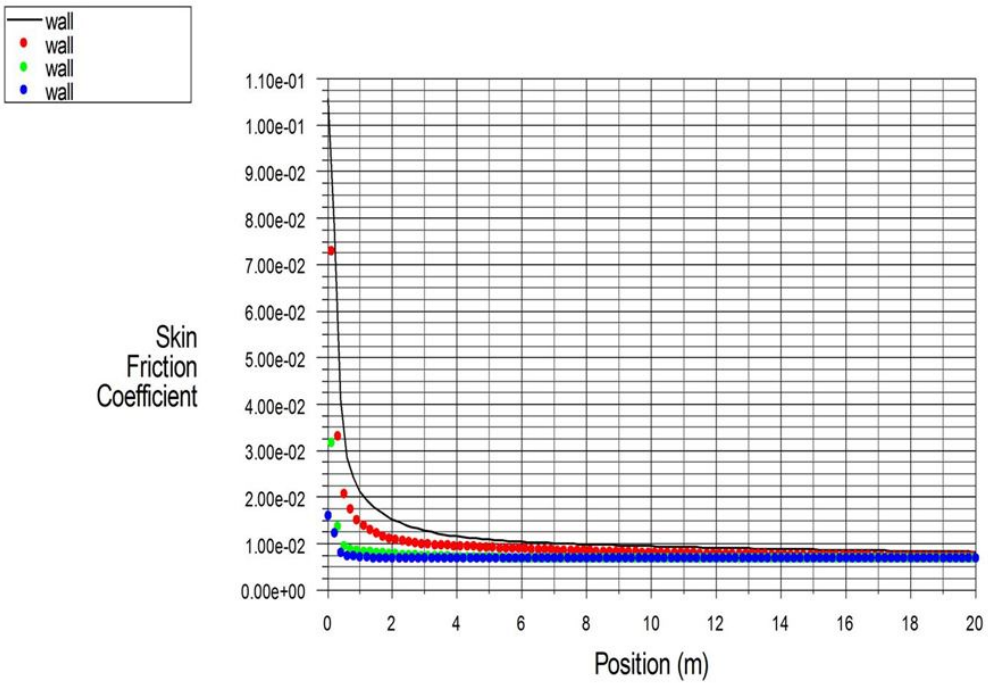

Figure 5.5 (a): Skin Friction Coefficient (i) D = 0.25m (blue) (ii) D = 1m (green) (iii) D = 5m (red) and (iv) D = 10m (black) for $k-\varepsilon$ model

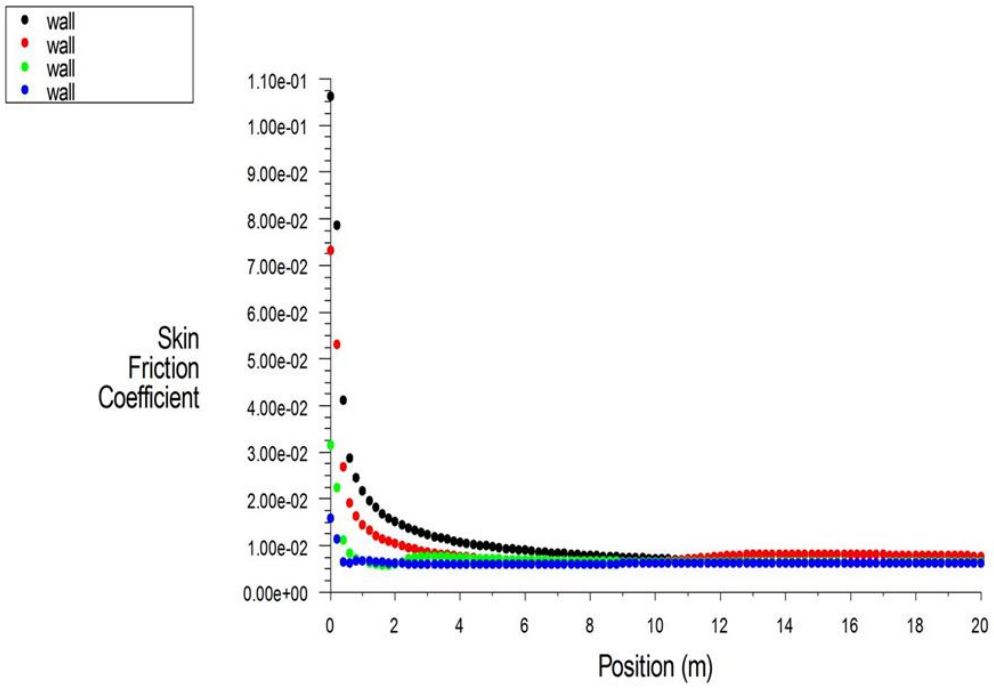

Figure 5.5 (b): Skin Friction Coefficient (i) D = 0.25m (blue) (ii) D = 1m (green) (iii) D = 5m (red) and (iv) D = 10m (black) for $k-\omega$ model.

In Fig.5.5 (a) the C_f profiles along the pipes for all the four diameters show similar trends .At the inlet, (i) and (ii) drop from 0.016 and 0.0325 respectively to 0.006 a meter away from the inlet and thereafter it remains steady to the outlet. (iii) drops from 0.073 to 0.008 and remains constant 6m away from the inlet. Also, (iv) drops sharply from 0.15 then remains constant at 0.009 8m away from the inlet.

In Fig. 5.5 (b) the C_f profiles along the pipes for all the three diameters are similar to those in the $k-\varepsilon$ model. At the inlet, (i) drops from 0.016 to 0.006, and after which it remains steady. Curve (ii) drops from 0.03 to 0.005 then slightly increases to 0.006, 3 meters away from the inlet where it remains constant. Similarly (iii) and (iv) drop from 0.075 and 0.108 respectively to 0.01, a distance 10m away from the inlet where it remains constant up to the outlet.

No significant differences are observed between results obtained with both models with similar corresponding boundary conditions. Results are almost unaffected by increasing the pipe diameters. For both models, as shown by figures 5.5 (a) and (b), values at the inlet are much higher and profiles have similar shape all along the lengths of the pipes. From the Moody chart the friction coefficient is given as 0.01. The wall shear stress is the highest at the pipe inlet where the thickness of the boundary layer is smallest and decreases gradually to the fully developed value. Therefore the pressure drop is higher in the entrance region of a pipe resulting in large velocity gradients and consequently larger wall shear stress. This zone is sensitive to initial conditions of flow imposed by flow geometry and Reynolds number effects.

Shear stress is caused by momentum flux due to the random motion of molecules and is largest at the wall. The shear stress acting between the wall and the first layer next to it results in a pressure and energy loss along the length of the pipe. The FLUENT near-wall model calculates wall shear stress based on the assumption that the law $u^+ = y^+$ exists in the viscous sublayer. Therefore, despite calculating approximately correct values of the mean velocity, a very minor inaccuracy may result in an erroneous local skin friction coefficient, C_f. As one moves away from the inlet, the C_f value decays exponentially. In a fully developed flow, the pressure gradient balances the wall shear stress only and attains a constant value as one moves away from the inlet.

5.6 Outlet Velocity Profile

Figures 5.6 (a) and (b) show the comparison of plotting the velocity at the outlet as a function of the distance from the center of the pipe with the following results:

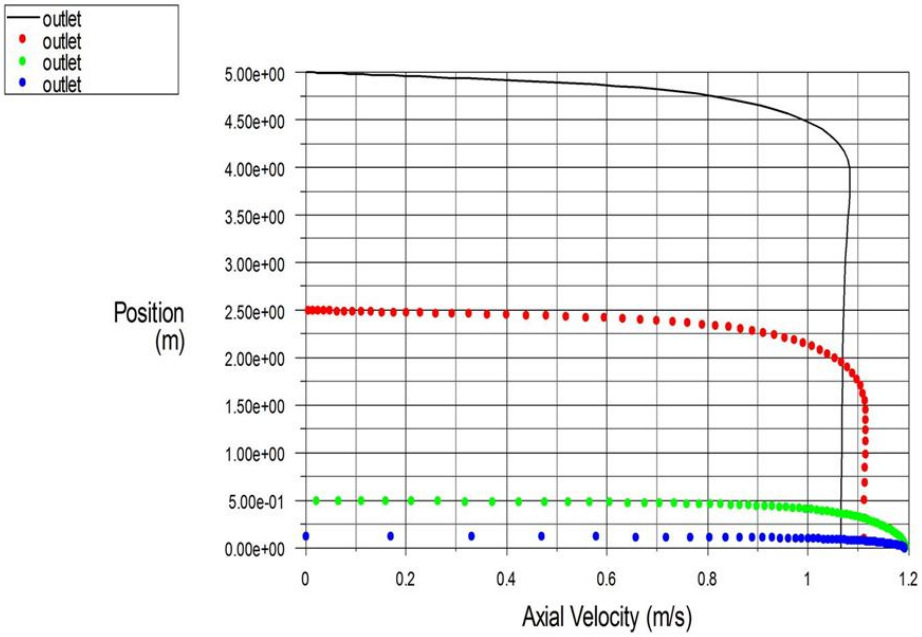

Figure 5.6 (a); Outlet Velocity Profile (i) D = 0.25m (blue) (ii) D = 1m (green) (iii) D = 5m (red) and (iv) D = 10m (black) for $k-\varepsilon$ model

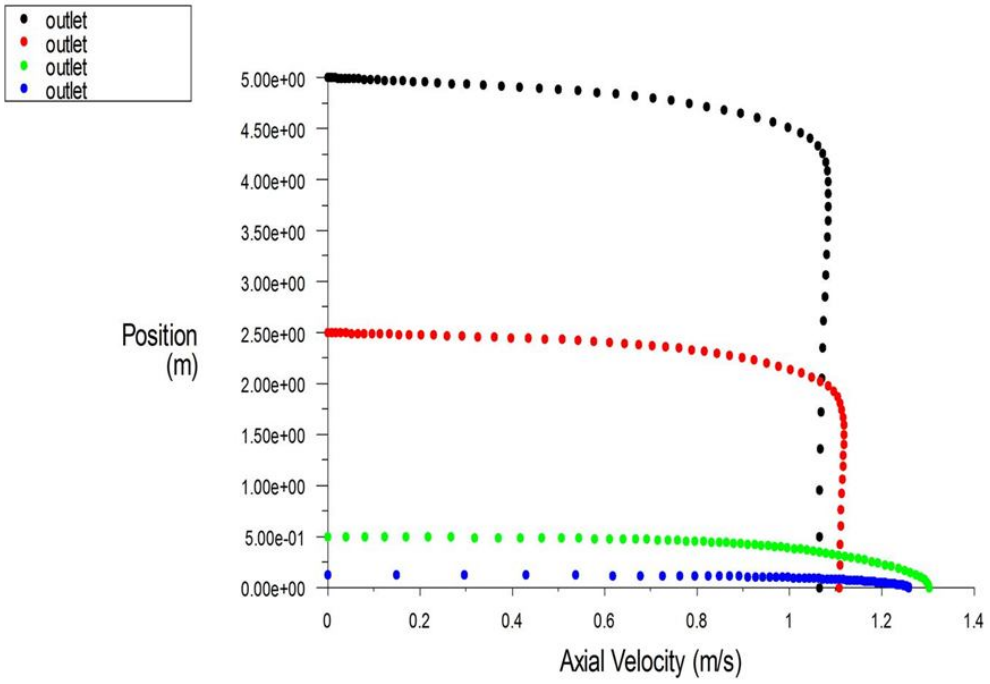

Figure 5.6 (b): Outlet Velocity Profile (i) D = 0.25m (blue) (ii) D = 1m (green) (iii) D = 5m (red) and (iv) D = 10m (black) for $k-\omega$ model

The axial velocity profiles in Fig.5.6 (a) for all the four pipes show a similar trend. They have a flattened shape at the wall corresponding to 0 velocity. As you move away from the wall, there is a slight increase in velocities for figures (i), (ii) up to 1.19m/s and 1.11m/s, 1.09m/s for figures (iii) and (iv) at the centerline respectively

In Fig. 5.6 (b),(i), the axial velocity is 0 m/s at the wall and this increases to 1.25m/s at the centerline. Figure (ii) has a 0 m/s velocity at the wall and this increases gradually to 1.3m/s at the centerline. Fig. (iii) and (iv) have a velocity of 0m/s at the wall, but this increases to 1.12m/s and 1.08m/s respectively at the centerline.

The axial velocity is maximum at the centerline and zero at the wall to satisfy the no-slip boundary condition for viscous flow. The region very close to the wall exhibits a nearly linear velocity profile because viscous effects are so dominant within this region. When a fluid is bounded by a solid surface, molecular interactions cause the fluid in contact with the surface to seek momentum and energy equilibrium with that surface. All fluids at the point of contact take on the velocity of that surface. Fluid adjacent to the wall sticks to the wall due to friction effect: There is very little activity, they turbulence level is very small and fluid velocity is nearly zero. The eddy motion loses its intensity close to the wall and diminishes at the wall because of the no-slip condition.

For both models the velocities at the centerline increase with a decrease in pipe diameter. The velocities are higher in the pipes diameter due small cross-sectional area and therefore viscous stresses dominate. The $k-\varepsilon$ model has a maximum value of 1.2m/s towards the centerline approximation compared to the theoretical value of 1.22 m/s. At the outlet, flow is fully developed and velocity is closer to uniform for all pipes.

5.7 Turbulent Intensity

The turbulence intensity, also often referred to as turbulence level, is defined as:

$$I = \frac{u'}{U} \tag{5.2}$$

where u' is the root-mean-square of the turbulent velocity fluctuations and U is the mean velocity.

When setting boundary conditions for a CFD simulation it is often necessary to estimate the turbulence intensity on the inlets. For flow in simple devices like large pipes, ventilation flows etc. or low speed flows the turbulence intensity is between 1% and 5%,, ANSYS FLUENT 12.1 Theory Guide, (2010). For fully developed pipe flow the turbulence intensity at the core can be estimated as:

$$I = 0.16\,\mathrm{Re}^{\frac{1}{8}} \tag{5.3}$$

Based on the Reynolds number, the Turbulent Intensities for the two models was set at 5%. Below are graphs showing the turbulent intensities along the various pipes:

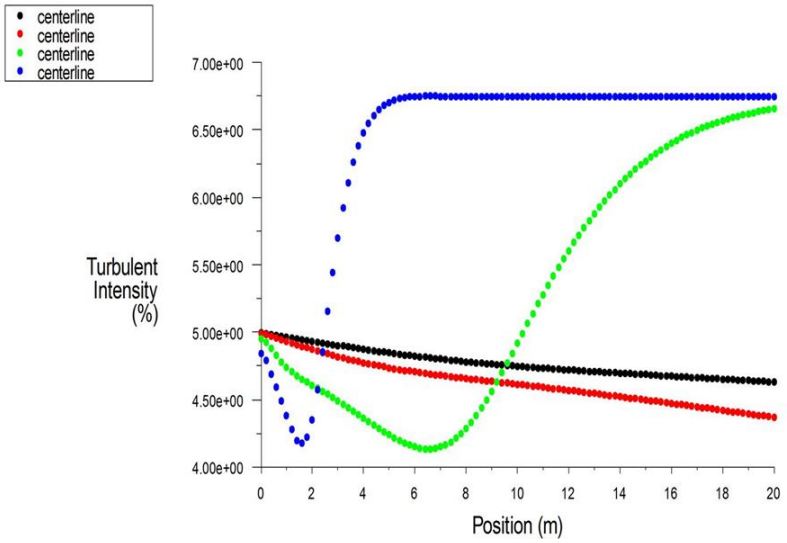

Figure 5.7 (a); Turbulent Intensity (i) D = 0.25m (blue) (ii) D = 1m (green) (iii) D = 5m (red) and (iv) D = 10m (black) for $k-\varepsilon$ model

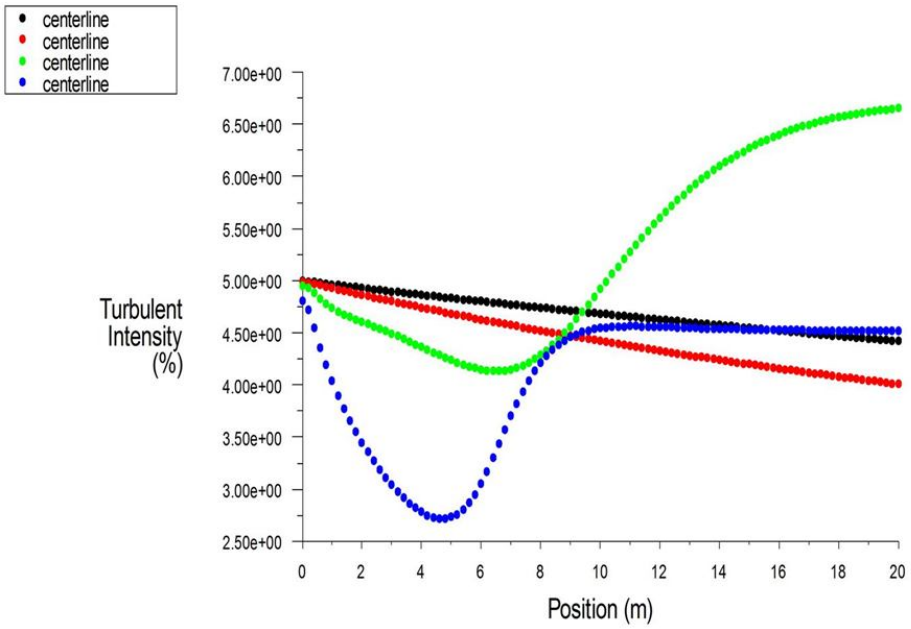

Figure 5.7 (b); Turbulent Intensity (i) D = 0.25m (blue) (ii) D = 1m (green) (iii) D = 5m (red) and (iv) D = 10m (black) for $k-\omega$ model

Figure 5.7 (a) and (b) demonstrate that the turbulent intensities decrease at the inlet for all the pipes up to some distance; Figure 5.6 (a) (i) and (ii) for the first 2m and 7m respectively. After these distances there is a rapid increase and the intensity goes beyond the set value of 5%. However for figures 5.6 (a) (iii) and (iv) the decrease is gradual throughout the length of the pipe. This decrease in turbulent intensity corresponds to an increase in velocity (fig 5.4 (a))

The behavior of the Turbulent intensities is similar for the $k-\omega$ except for D = 1m where it shoots up the inlet 5% value. The decrease along the pipe lengths corresponds to an increase in axial velocities as can be seen from figure 5.4 (b).

Over prediction of the $k-\varepsilon$ is attributed to the dumping function used in the model namely:

$\exp\left[\frac{-3.4}{(1+\mathrm{Re}_t/50)^2}\right]$ and $1-0.3\exp(-\mathrm{Re}_t)^2$, , ANSYS FLUENT 12.1 Theory Guide, (2010). where Re_t is the locale turbulent Reynolds' number. These terms are used to model turbulence right down to the wall where viscous effects dominate. Because of the variation, the dumping function is not able to detect the near wall characteristics correctly. The $k-\omega$ predictions are better owing to the fact that in this model, the dumping function used is unity and does not depend on the local turbulent Reynolds' number.

5.8. Validation

The following graphs show comparisons of centerline velocity. Coefficioent of skin friction and outlet velocity on two different meshes; Unrefined (30 x 100) and refined (60x100).

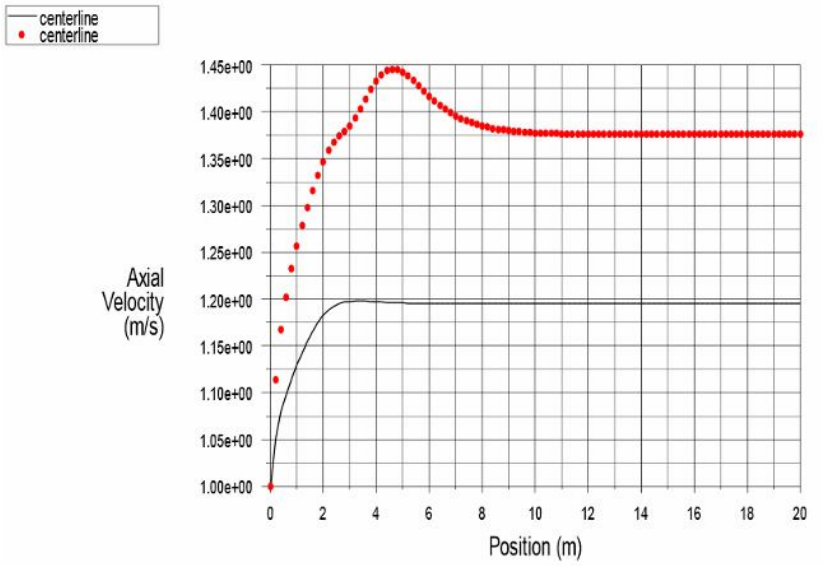

Figure 5.8 (a); Axial velocity for D = 0.25m for refined (red) and unrefined (black) for $k-\varepsilon$ model

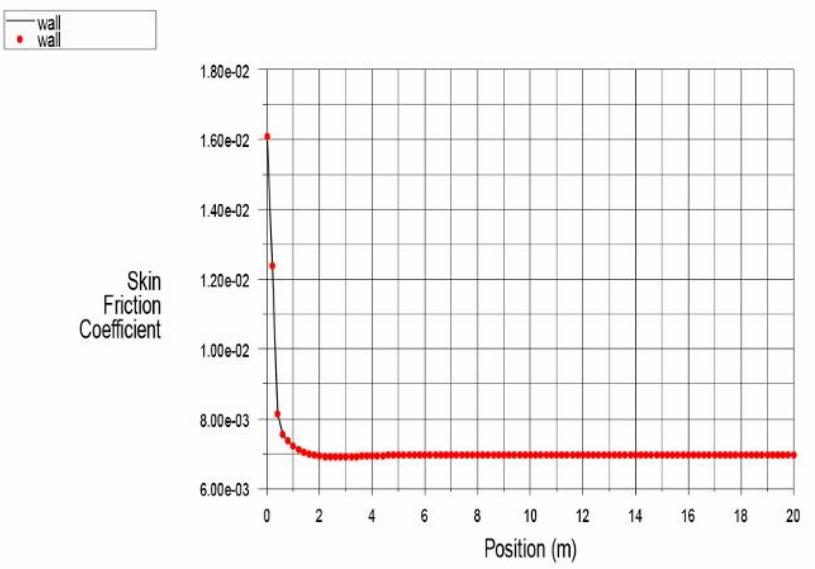

Figure 5.8 (b); Skin Friction coefficient for D = 0.25m for refined (red) and unrefined (black) for $k-\varepsilon$

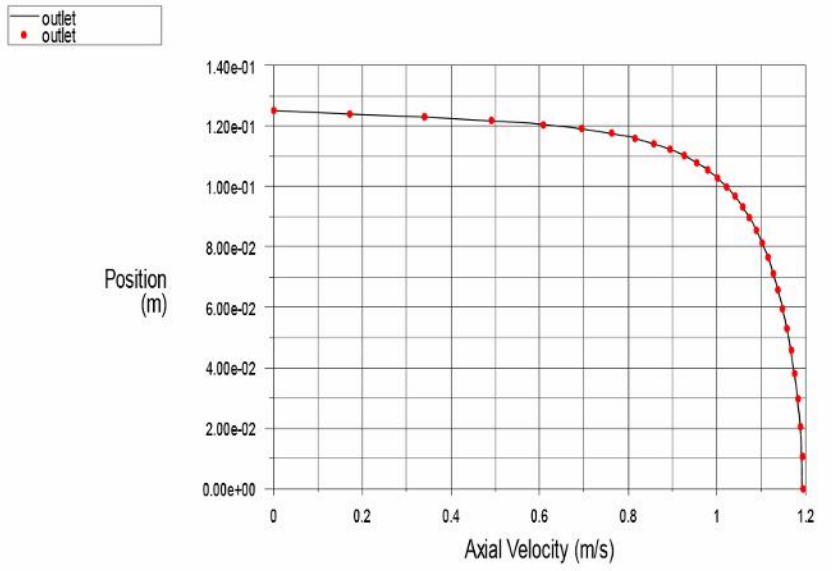

Figure 5.8 (c); Outlet velocity profile for D = 0.25m for refined (red) and unrefined (black) for $k-\varepsilon$

From the above three plots the skin friction and outlet velocity profile have remained nearly unchanged. However the centerline velocity results show significant improvement with the refined mesh.

CHAPTER SIX

CONCLUSION AND RECOMMENDATION

In this chapter, conclusions regarding the relative performance of the two models are given. The conclusions here are based on the results discussed in chapter five.

6.1 Conclusions

The purpose of this study has been to analyze the turbulent flow inside pipes of varying diameters using two equation RANS $k-\varepsilon$ and $k-\omega$ models at a constant Reynolds number. Numerical results were obtained for the two models for velocity, skin friction coefficient and Turbulent Intensity along the length of the pipes.

(i) Axial velocity increases along with the length of pipe and in the fully developed regime it becomes constant.

(ii). The velocities at the centerline increase with a decrease in pipe diameter

(iii).The turbulent intensities show a decrease at the inlet. This decrease in turbulent intensity corresponds to an increase in velocity.

(iv).Skin friction coefficient decreases along with the length of pipe and becomes constant after entering the fully developed regime.

(v).The axial velocity is maximum at the centerline and zero at the wall to satisfy the no-slip boundary condition for viscous flow.

(vi).The $k-\varepsilon$ model gives better approximation for the centerline velocities. The results compare relatively well in terms of the entry length of the pipes.

(vii). The $k-\varepsilon$ model is more suitable for predicting turbulent flow in a pipe.

From the study the following conclusions are made:

(i). For good parametric studies and some unconfined flow problems where certain degree of generality are required we recommend $k-\omega$ model to be used.

(ii).In situations where boundary value problems and for many industrially relevant flows the $k-\varepsilon$ model is recommend. It is well established and most widely validated turbulence model.

6.2 Suggestions for further study

(i). In this study we recommended the $k-\varepsilon$ for many industrially relevant flows because it is most widely validated. Do more studies using the $k-\omega$ model so that it can become established.

(ii).A study can be carried out with fluid entering the pipe with pipe walls at different temperature from fluid temperature.

(iii).The effect of variable properties to be studied while varying the length of the pipes at constant Reynolds number.

(iv).The results obtained in this study can be compared with results obtained using other two- equation models like SST , LES in fluent.

(v). This study can be done using a different software or using a different method like the finite difference.

(vi). Study of pipes of a different cross-sectional area geometry for example rectangular, triangular and so on.

REFERENCES

Adrian Bejan, (1994),"Convective Heat Transfer", John Wiley and Sons,

Anderson D. J, (1995), "Computational fluid dynamics, First edition".

ANSYS FLUENT 12.1 "Theory Guide", (2010).

Bhandari D. and Singh S., (2012), "Analysis of fully developed turbulent flow in a pipe using Computational fluid dynamics", *International Journal of Engineering Reasearch and Technology*, **1**: 2278-0181.

Banfi G.P., De Micheli R.and Henin A., (1981), "Velocity fluctuation enhancement in the transition to turbulence in a pipe", *Journal of Physics D: Applied Physics*, **14**: 625-632.

Barth T. J. and Jespersen D., (1989), "The design and application of upwind schemes on unstructured meshes". *AIAA-**89**-0366*, AIAA 27th Aerospace Sciences Meeting, Reno, Nevada.

Bell B., (2003), "Turbulent flow cases", Fluent Inc.

Bloor M. S., **(**1964), "The transition to turbulence in the wake of a circular cylinder", *Journal of Fluid Mechanics*, **9:** 290-304.

Boussinesq, J., (1877), "Théorie de l'Écoulement Tourbillant", Mem. Présentés par Divers Savants Acad. Sci. Inst. Fr., **23**: 46-50.

Boussinesq J., (1877), "Essai sur la th´eorie des eaux courantes", M´em. pr´es. par div. savant `a l'Acad.Sci. **23** : 1–680.

Chen H. C. and Patel V. C., (1988), "Near-Wall Turbulence Models for Complex Flows Including Separation", *AIAA Journal*, **6**:641-648.

Christoph G.H. and Pletcher R.H., (1971), "Prediction of Roughwall-Skin friction and Heat transfer". *AIAA Journal*

Cole M., (1999), "*Disturbance of Flow Regimes by Jet Induction"*, Ph.D. Thesis, Victoria University of Technology, Australia.

Deardorff J. W., (1970), "A numerical study of three-dimensional turbulent channel flow at Large Reynolds numbers", J. Fluid Mech. **41**: 453.

Ferrey P. and Aupoix B., (2006), "Behaviour of turbulence models near a turbulent/nonturbulent interface revisited", *Journal of Heat and Fluid Flow*, **27**: 831-837.

Germano M., Piomelli U, Moin P. and Cabot W. H., (1991), "A dynamic subgrid-scale eddy viscosity model", Phys. Fluids A **3** : 1760–1765.

Hinze J. O., (1984)," Turbulence", McGraw-Hill, New York.

Huang P., Bradshaw P., and Coakley T., (1993), "Skin Friction and Velocity Profile Family for Compressible Turbulent Boundary Layers". *AIAA Journal*, **9**:1600-1604.

Jones D. A. and Clarke D. B., (2008). "Simulation of flow past a sphere using the Fluent code", Published by Maritime Platforms Division, DSTO Defense Science and Technology Organization, Australia.

Jongen T., (1992), "*Simulation and Modeling of Turbulent Incompressible Flows*", Ph.D thesis, EPF Lausanne, Lausanne, Switzerland.

Jurij S., (2007), "Turbulence models in CFD", University of Ljubljana.

Kader B., (1981), “Temperature and Concentration Profiles in Fully Turbulent Boundary Layers”. *Int. J. Heat Mass Transfer*, **9**:1541-1544

Kolmogorov A. N., (1941), “The local structure of turbulence in incompressible viscous fluid for very large Reynolds number”, Dokl. Acad. Nauk. SSSR **30**: 9–13.

Kolmogorov A. N., (1942), “Equations of turbulent motion of an incompressible turbulent fluid”, Izv.Akad. Nauk. SSSR Ser. Phys. **I**: 1–2.

Kraichnan R. H., (1958), “Irreversible statistical mechanics of incompressible hydromagnetic turbulence”, Phys. Rev. **109**: 1047.

Launder B. E. and Spalding D. B., (1972), “Mathematical models of turbulence”, Departments of Mechanical Engineering, Imperial College of Science and Technology, London, England

Launder B. E. and Spalding D. B., (1972), “Mathematical Models of Turbulence”, Academic Press.

Launder B. E. and Sharma B. I., (1974), “Application of the energy dissipation model of turbulence to the calculation of flow near a spinning disc”, Letters in Heat and Mass transfer, **1**: 131– 138.

Launder B. E. and Spalding D. B., (1974), “The Numerical Computation of Turbulent Flows”. Computer Methods in Applied Mechanics and Engineering, **3**:269-289.

Lorenz E. N., (1963). “Deterministic non-periodic flow”. *J. Atmos. Sci.***20**: 130–141.

Menter F.R., (1992), "Improved Two-equation $k-\omega$ Turbulence Models for aerodynamic flows". NASA TM-103975

Menter F.R., (1994), "Zonal Two-equation $k-\omega$ Turbulence Models for aerodynamic flows". *AIAA* **93**: 2906.

Mullin T. and Peixinho J., (2006), "Transition to Turbulence in pipe flow", *Journal of Low Temperature Physics*, **145:** 75-88.

Orszag S. A. and Patterson G. S., (1972), "Numerical simulation of turbulence: statistical models and turbulence", Physics **12**: 127–147, Springer-Verlag, Berlin.

Patankar S. V., (1980), "Numerical Heat Transfer and Fluid Flow Hemisphere", Washington D.C.

Peng S.H., Davidson L. and Holmberg S., (1997), "A modified low-Re number $k-\omega$ for Recirculating flows", *ASME journal of fluids Engineering*. **119**, 867-875.

Pepper D. W. and Carrington David, (2009), "Modeling indoor air pollution, First edition", Singapore.

Piomelli U., (1993), "High Reynolds number calculations using the dynamic subgrid scale Stress model", Phys. Fluids A **5**: 1484–1490.

Prandtl, L. (1925). "Bericht über Untersuchungen zur ausgebildeten Turbulenz", *Z.* Angew.Math, Meth. **5**: 136-139.

Prandtl L., (1932), "Zur turbulenten Stroemung in Rohren und laengs Platten. Ergeb. Aerodyn.Versuch"

Reynolds O., (1895), “On the dynamical theory of incompressible viscous fluids and the determination of the criterion”, Phil. Trans. Roy. Soc. London Ser. A **18**:123-164.

Rudman M., Graham L. J., Blackburn H. M. and Pullum L., (2002), Non-“Newtonian Turbulent And Transitional Pipe Flow”. Presented at Hy15, Banff, Canada.

Saffman P. G., (1970), “The velocity of viscous vortex rings”. Stud. Appl. Maths.**49**, 371–380.

Saffman P.G. and Wilcox D.C, (1974), “Turbulent model predictions for Turbulent boundary Layers”. *AIAA*, **12**: 541-546.

Sahu M., Kishanjit K. K. ,Kanhu C. P. and Naik T., (2009),” Developed laminar flow in pipe using computational fluid dynamics”, 7th International R & D Conference on Development and Management of Water and Energy Resources, Bhubaneswar, India.

Smagorinsky J., (1963), “General Circulation experiments with the primitive equations”, The basic experiment, Month. Weath. Rev. **91**: 99–165.

Speziale C.G, Gatski T.B. and Mac Giolla Mhuiris N., (1990), “Phys. Fluids” A **2**: 1678-1684.

Tannehill J.C., Anderson D.A, Richard H., (1997), “Computational fluid mechanics and heat transfer, second edition”, Taylor and Francis, London.

Taylor G. I., (1935), “Statistical theory of turbulence”, Proc. Roy. Soc. London A**151**: 421– 478.

Taylor N.A.,(1984) ,” Modeling of Air Flows Through the Sample Pipe of a Smoke Detecting System”, United Kingdom Atomic Energy Authority.

Versteeg H. K.and Malalasekera W., (2007),” An introduction to computational fluid dynamics,second edition”, Prentice Hall, England.

Von K´arm´an T., (1937), “On the statistical theory of turbulence”, Proc. Nat. Acad. Sci., Wash. **23**: 98.

Turbulent Skin Friction Under Arbitrary Conditions”, Technical Report AFFDL-TR-70-133.

White F. M., (1974), “Viscous fluid flow, First edition”. Printed in USA.

Wilcox D. C., (1988), “Reassessment of scale determining equation for advanced turbulence Models”, *AIAA J.*, **26** 1299-1310.

Wilcox D. C., (1998), “Turbulence Modeling for CFD”, DCW Industries, Inc., La Canada California.

Wilcox D. C., (2004), “Turbulence modeling for CFD, Second edition”, Printed in the California.

Wilcox D. C. and Rubesin M.W.,(1980), “Progress in turbulence modelling for complex flow fields including effects of compressibility”, *NASATP*, **486:**1517.

Wilcox D. C. and Traci R.M., (1976), “A complete model of Turbulence”, *AIAA pr* 76-351, San Diego, CA.

Willis A. P, Peixinho J., Kerswell R.R. and Mullin T. (2008), “Experimental and theoretical progress in pipe flow transition”, Phil. Trans. Roy.Soc A **366**: 2671-2684

Yogini Patel, (2010), “*Numerical Investigation of Flow Past a Circular Cylinder and in a Staggered Tube Bundle Using Various Turbulence Models”*, M.Sc Lappeenranta University of Technology

Zdravkovich M. M., (1997), “Flow around circular cylinders fundamentals, First edition”, Printed in Oxford University Press, New York.

Zevenhoven Ron, (2009), “Introduction to computational fluid dynamics. Heat Engineering Laboratory”, Ĺbo Akademi University, Finland.

APPENDIX

A. APPENDIX 1: First publication

MATHEMATICAL ANALYSIS OF TURBULENT FLOW IN PIPES OF VARYING DIAMETERS USING RANS $k-\varepsilon$ MODEL

[1]B.K. Menge, [2] M. Kinyanjui, [3]J.k.Sigey

[1]Department of Mathematics and Physics. Technical University of Mombasa, P.O BOX 90420-80100,Mombasa, Kenya. bethmenge@gmail.com

[2,3]Department of Pure and Applied Mathematics, Jomo Kenyatta University of Agriculture and Technology, Box 62000-00200, Nairobi, Kenya

Abstract

In analysing fluid flow problems, Computational Fluid Dynamics based simulation procedures are now considered to be an indispensable analysis and design tool in a wide and ever-increasing range of applications involving fluid flow. In the analysis of water distribution networks, the design parameters are the lengths, diameters, and the coefficients of friction of a pipe. This paper presents computational investigation of turbulent flow inside pipes of varying diameters. Reynold's Averaged Navier Stokes Turbulent model; the $k-\varepsilon$ model is used for the simulation. The Reynolds number based on the pipe diameter and average velocity at the inlet is 10,000.

The fluid used for this purpose is air with Pr = 0.7 and the pipe material is aluminium. The fluid used for this purpose is air. The results obtained computationally are well in agreement with the results obtained experimentally.

Keywords: *Computational fluid dynamics, Reynold's Averaged Navier Stokes,* $k-\varepsilon$ *model, Turbulent, Average Velocity, Coefficient of friction.*

Nomenclature

C_f Skin friction coefficient

D Diameter of Pipe, m

f Friction factor

I Turbulent intensity

L Length of Pipe, m

n Function of the Reynolds number

P Pressure

Q Volume flow rate, m^3/s

r Radius of elementary ring

R Radius of pipe, m

Re Reynolds number

Pr Prandtl number

U mean velocity

V_c centerline velocity m/s

v velocity at the inlet m/s.

τ_w Wall shear stress

ρ Density of fluid kg/m^3

u' root-mean-square of the turbulent velocity fluctuations

u_i, u_j Mean velocities of fluid

μ Dynamic viscosity

1.0 Introduction

Fluid flow is classified as external and internal, depending on whether the fluid is forced to flow over a surface or in a conduit. The transport of fluid in a closed conduit is extremely important in our daily operations. A brief consideration of the world around us will indicate that there is a wide variety of applications of pipe flow. The hot and cold water that we use in our homes is pumped through pipes. Water in a city is distributed by extensive piping networks. Oil and natural gas are transported hundreds of miles by large pipelines. Blood is carried throughout our bodies by arteries and veins. The cooling water in an engine is transported by hoses to the pipes in the radiator where it is cooled as it flows. Thermal energy in a hydronic space heating system is transferred to the circulating water in the boiler, and then it is transported to the desired locations through pipes. The analysis of pipe flow is also very important from the engineering point of view. Due to rigorous engineering application and implications, it has become quite necessary to carry out an analysis on the nature of flow inside pipes and tubes. The objective of the present work is to investigate the nature of fully developed turbulent flow in a pipe computationally and to determine the various parameters such as skin friction coefficient, axial velocity, turbulent intensity and centerline velocity associated with it. Although some of these parameters such as the pipe lengths and the pipe diameters would remain the same at different points but the coefficients of friction would change during the life of network and therefore they can be treated as imprecise information

One important characteristics of a turbulent flow is that the velocity and pressure may be steady or remain constant at a point, but still may exhibit irregular fluctuations over the mean or average value. The fluid elements which carry out fluctuations both in the direction of main flow and at right angles to flow are not individual molecules but rather are lumps of fluid of varying sizes known as eddies

In the computational simulation of turbulent flow, it is important to decide how finely we should resolve theses eddies in the computational model as it has a direct effect on the accuracy of the prediction as well as computer time. Methods available for simulating turbulent fluid flow are Direct Numerical Simulation (DNS*)* based on direct solution of Navier-Stokes Equations and Averaged or Filtered Simulation based on averaged solution of Navier-Stokes Equations.

In principle, the time dependent three dimensional Navier-Stokes equations can fully describe all the physics of a given turbulent flow. For a general linear Newtonian viscous fluid the Navier-Stokes equations are given by the following set of equations:

$$\frac{\partial \rho}{\partial t} + \frac{\partial}{\partial x_i}(\rho u_i) = 0 \tag{1}$$

$$\frac{D(\rho u_i)}{Dt} = \rho g - \nabla P + \frac{\partial}{\partial x_j}\left[\mu\left(\frac{\partial u_i}{\partial x_j} + \frac{\partial u_j}{\partial x_i}\right) + \delta_{ij}\lambda\, div V\right] \tag{2}$$

1.1 Literature Review

A large number of research analysis have been carried out on the internal flows during the recent years. Sahu *et al* (2009) investigated the accuracy of numerical modelling of the laminar equation to determine the friction factor of pipe. They found the friction factor to be 0.0151 at the entrance length of 2.7068 m. while the experimental result shows the value of friction factor as 0.0157.

Banfi *et al* (1981) used a laser-Doppler velocimeter to investigate transitional pipe flow, in particular the behavior of the velocity fluctuations as the Reynolds number was increased from 1500 to 4000. It was noted that the velocity fluctuations reached a maximum at a Reynolds number of about 2800 (in the transition region). Rudman *et al* (2002) compared results from experimental and numerical investigations of non–Newtonian fluids at transition to turbulence and in weakly turbulent flows. Experimental results showed flow features similar to turbulent puffs and slugs observed in Newtonian transitional flows. Numerical results showed some quantitative discrepancies with the experimental results but did show turbulence suppression, drag reduction and delayed transition as observed experimentally. Yogini P. (2010) carried out a numerical simulation of flow past a circular cylinder, using a commercial CFD code (ANSYS Fluent 12.1) with large eddy simulation (LES) and RANS Shear-Stress Transport (SST) approaches for Reynolds 1000 and 3900. The numerical results extracted from these simulations have good agreement with the experimental data of Zdravkovich M.M. (1997).

1.2 Pre-analysis

A turbulent flow exhibits small-scale fluctuations in time. It is usually not possible to resolve these fluctuations in a CFD calculation. So the flow variables such as velocity, pressure, etc. are time-averaged. Unfortunately, the time-averaged governing equations are not closed. (that is, they contain fluctuating quantities which need to be modeled using a turbulence model.)

The k-ε models consist of two differential equations: one each for the turbulent kinetic energy k and turbulent dissipation ε. These two equations have to be solved along with the time-averaged continuity, momentum and energy equations. To obtain the equations that govern the current problem, the following assumptions are made for the analysis:

(i). Constant transport properties of fluid

(ii). Incompressible fluid flow

(iii). Newtonian fluid

(iv). continuum fluid.

1.3 Computational domain

The computational domain and the boundary conditions for the simulation of the flow are shown in Figure 1. The cylinder is simulated with a diameter (D) and length L. This paper will consider the flow inside pipes of varying diameters and a length of 20m using FLUENT 6.3.26. The geometry is symmetric therefore we will model only half portion of the pipe (radius R).

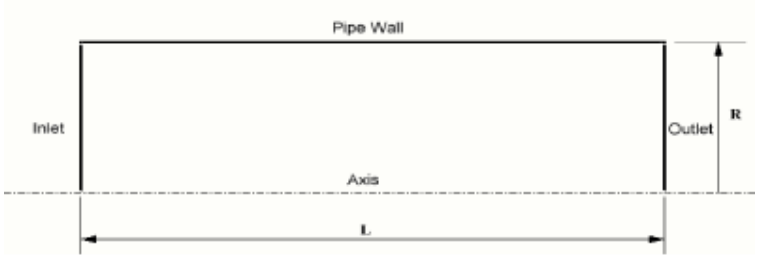

Figure 1: computational geometry

Air enters from the inlet boundary with a velocity of 1m/s and various viscosities μ depending on the diameter of the pipe. The flow Reynolds number is 10,000 to illustrate the turbulent flow.

1.4 Simulation set-up

The analysis is carried out with the help of CFD package FLUENT 6.3.26 which is a computational fluid dynamics (CFD) software package to simulate fluid flow problems. It uses the finite volume method to solve the governing equations for a fluid. Geometry and grid generation is done in GAMBIT 2.3.16 which is the preprocessor bundled with FLUENT.

In this 2D-code, discretization is done based on a finite volume approach. A steady and pressure based solver is used. A least square cell based method is used to calculate gradients. Boundary conditions and the discretization schemes used are summarized in Table 1 below. We have considered convergence criteria $1x10^{-6}$ for these simulations.

Table 1: Simulation settings for flow in a pipe with RANS $k-\varepsilon$ model

Settings	Choice
Simulation type	2D, Steady
Space	Axisymmetric
Solver	Double precision, pressure based and implicit
Temporal disretization	2nd order
Turbulence model	$k-\varepsilon$ model
Pressure	Standard
Pressure-velocity coupling	SIMPLE
Momentum	2nd order upwind
Turbulent kinetic energy	2nd order upwind
Turbulent dissipation rate	2nd order upwind
Boundary conditions:	
Inlet	Velocity inlet
Outlet	Pressure outlet
Top wall	No-slip wall
Bottom wall	Axis

1.5 Turbulent velocity profile

The velocity profile for turbulent flow through a smooth pipe is approximated by the power-law equation :

$$\frac{u}{V_c} = \left(1 - \frac{r}{R}\right)^{\frac{1}{n}} \tag{3}$$

Where u is the time mean average of x- component of instantaneous velocity, V_c is the centerline velocity or axial velocity, R is the radius of pipe, r is the radius of elementary ring and n is a function of the Reynolds number. To determine the

centerline velocity V_c, we must know the relationship between V (the average velocity) and V_c . This can be obtained by integration of equation (3). Since the flow is axisymmetric,

$$Q = AV = \int udA = V_c \int_{r=0}^{r=R} \left(1 - \frac{r}{R}\right)^{1/n} (2\pi r) dr \tag{4}$$

$$Q = 2\pi R^2 V_c \frac{n^2}{(n+1)(2n+1)} \tag{5}$$

Since $Q = \pi R^2 V$, we get

$$\frac{V}{V_c} = \frac{2n^2}{(n+1)(2n+1)} \tag{6}$$

1.6 Results and Discussion

In this section we will discuss the cases with D = 0.25m, D = 1m, D=5m and D = 10m respectively. Here all simulations have been done using a grid which contains 6000 quadrilateral cells.

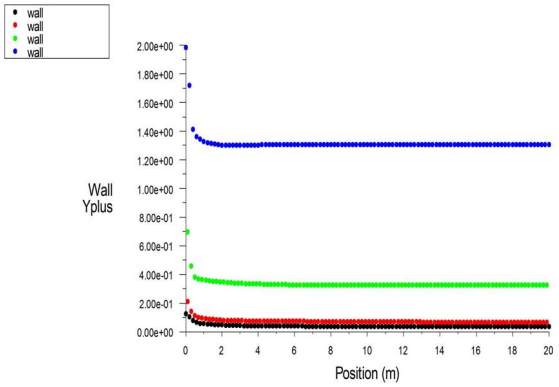

Figure 2:Wall Y plus : (i) D = 0.25m(blue) (ii) D = 1m(green) (iii) D = 5m(red) and (iv) D = 10m(black) for $k-\varepsilon$ model

There is a sharp drop in the y^+ values for all the three pipes at the inlet. For all cases the y^+ is seen to be < 5 therefore the near-wall grid resolution is acceptable. For all the four pipes it can be observed that there are no changes in these profiles with time, that is away from the inlet.

Axial velocity

We plot the axial velocity as a function of the distance along the centerline of the pipe

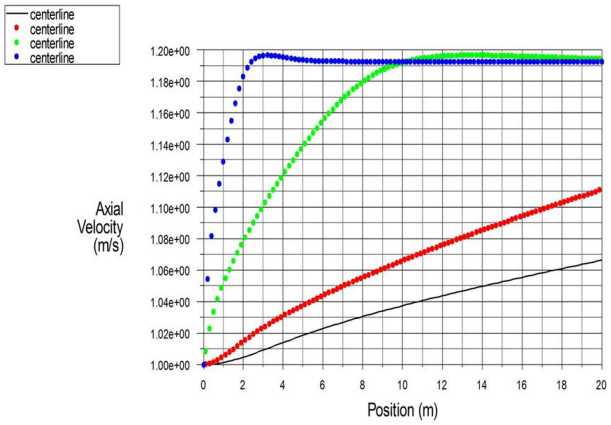

Figure 3: Axial velocity (i) D = 0.25m(blue) (ii) D = 1m(green) (iii) D = 5m(red) and (iv) D = 10m(black) for $k-\varepsilon$ model

In fig 3 (i) and (ii), the velocity reaches a constant value beyond a certain distance from the inlet: x = 6m and x = 11m respectively. This is the fully-developed flow region where the centerline velocity becomes a constant. Fig (iii) and (iv) shows the velocity increasing steadily from 1m/s to 1.11m/s and 1.09m/s respectively at the outlet.

The flow rate decreases when the diameter is increased as can be seen from the figures except for the pipe with the smallest diameter. Flow towards center of the

pipe tends to flow faster in the flow direction. When a fluid is bounded by a solid surface, molecular interactions cause the fluid in contact with the surface to seek momentum and energy equilibrium with that surface. All fluids at the point of contact take on the velocity of that surface. As the flow develops downstream of the inlet, the boundary layer grows, the fluid near the wall is retarded by viscous friction and this results in an injection of fluid into the region away from the wall to satisfy mass conservation.

Skin Friction Coefficient

The value of skin friction coefficient is given by

$$C_f = \frac{\tau_w}{\frac{1}{2}\rho V^2} \tag{7}$$

where τ_w is the Wall shear stress and is given by

$$\tau_w = \frac{\Delta p D}{4L} \tag{8}$$

The pressure drop Δp is given by

$\Delta p = f \frac{L}{D} \frac{\rho V^2}{2}$, where f is the friction factor and is calculated with the help of the Moody chart.

Plotting the friction coefficient along the top wall gives the following results:

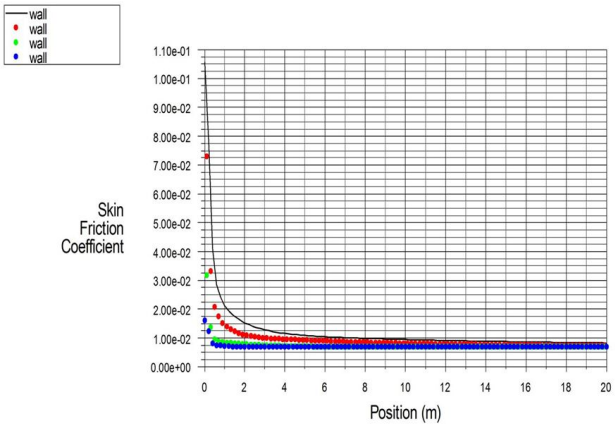

Figure 4: Skin Friction Coefficient (i) D = 0.25m(blue) (ii) D = 1m(green) (iii) D = 5m(red) and (iv) D = 10m(black) for $k-\varepsilon$ model

In Fig4 the C_f profiles along the pipes for all the four diameters show similar trends. As one moves away from the inlet, the C_f value decays exponentially. Shear stress is caused by momentum flux due to the random motion of molecules and is largest at the wall. In a fully developed flow, the pressure gradient balances the wall shear stress only and attains a constant value as one moves away from the inlet.

Velocity Profile

Plotting the velocity at the outlet as a function of the distance from the center of the pipe:

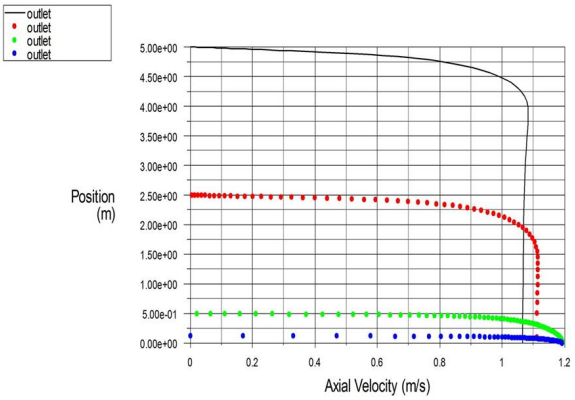

Figure 5; Velocity Profile (i) D = 0.25m(blue) (ii) D = 1m(green) (iii) D = 5m(red) and (iv) D = 10m(black) for $k-\varepsilon$ model

The axial velocity profiles in Fig.5 for all the four pipes show a similar trend. They have a flattened shape at the wall corresponding to 0 velocity. As you move away from the wall, there is a slight increase in velocities for figures (i), (ii) up to 1.19m/s and 1.11m/s,1.09m/s for figures (iii) and (iv) at the centerline respectively.

The axial velocity is maximum at the centerline and zero at the wall to satisfy the no-slip boundary condition for viscous flow. The velocities at the centerline increase with a decrease in pipe diameter

Turbulent Intensity

The turbulence intensity, also often referred to as turbulence level, is defined as:

$$I = \frac{u'}{U} \tag{9}$$

For fully developed pipe flow the turbulence intensity at the core can be estimated as:

$$I = 0.16Re^{\frac{1}{8}} \tag{10}$$

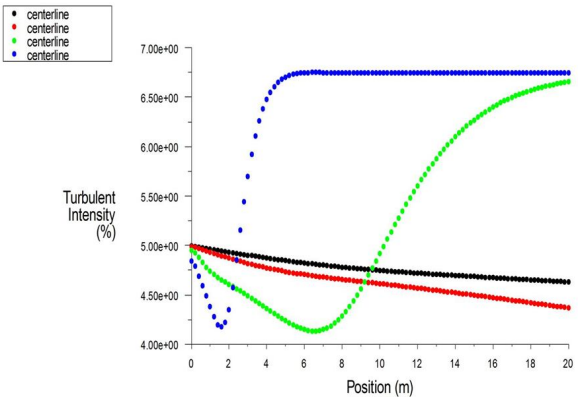

Figure 6:Turbulent Intensity (i) D = 0.25m(blue) (ii) D = 1m(green) (iii) D = 5m(red) and (iv) D = 10m(black) for $k-\varepsilon$ model

The turbulent intensities show a decrease at the inlet for all the pipes upto some distance; Figure (i) and (ii) for the first 2m and 7m respectively. After these distances there is a rapid increase and the intensity goes beyond the set value of 5%. However for figures (iii) and (iv) the decrease is gradual throughout the length of the pipe. This decrease in turbulent intensity corresponds to an increase in velocity (fig 3)

1.7 Conclusion

Based on the CFD analysis of the flow inside the pipe the following conclusions can be drawn:

1. The velocities at the centerline increase with a decrease in pipe diameter

2. Axial velocity increases along with the length of pipe and in the fully developed regime it becomes constant.

3. The turbulent intensities show a decrease at the inlet. This decrease in turbulent intensity corresponds to an increase in velocity.

4. Skin friction coefficient decreases along with the length of pipe and becomes constant after entering the fully developed regime.

5. The axial velocity is maximum at the centerline and zero at the wall to satisfy the no-slip boundary condition for viscous flow

1.8 References

[1] ANSYS FLUENT 12.1 Theory Guide, (2010).

[2].G. P. Banfi, R. De Micheli, A. Henin, Velocity fluctuation enhancement in the transition to turbulence in a pipe., *Journal of Physics D: Applied Physics* **14**, 625-632(1981). *M.* [3] M. Rudman, L. J. Graham, H. M. Blackburn, L. Pullum *Non-Newtonian Turbulent and Transitional Pipe Flow.* Presented at Hy15, Banff, Canada, 2002

[4] M. Sahu, Kishanjit Kumar Khatua and Kanhu Charan Patra, T. Naik, Developed laminar flow in pipe using computational fluid dynamics, 2009,*7th International R & D Conference on Development and Management of Water and Energy Resources, 4-6 February2009, Bhubaneswar, India*

[5] Yogini Patel (2010) Numerical Investigation of Flow Past a Circular Cylinder and in a Staggered Tube Bundle Using Various Turbulence Models. *M.Sc* Lappeenranta University of Technology

[6] Zdravkovich, M. M., (1997). Flow around circular cylinders Vol 1: fundamentals , First edition. Printed in Oxford University Press, New York.

B. APPENDIX 2: Second publication

A COMPARATIVE ANALYSIS OF TURBULENT PIPE FLOW USING $k-\varepsilon$ AND $k-\omega$ MODELS.

[1]B.K. Menge, [2] M. Kinyanjui, [3]J.k.Sigey

[1]Department of Mathematics and Physics. Technical University of Mombasa, P.O BOX 90420-80100,Mombasa, Kenya. bethmenge@gmail.com

[2,3]Department of Pure and Applied Mathematics, Jomo Kenyatta University of Agriculture and Technology, Box 62000-00200, Nairobi, Kenya

Abstract

Many if not most flows of engineering significance are turbulent. Fluid engineers need access to viable tools capable of representing the effects of turbulence. In this paper, a computational fluid dynamics model of fully developed turbulent flow in the pipes is implemented with the help of ANSYS FLUENT 6.3.26 software and its preprocessor Gambit 2.3.16. Two Reynolds Averaged Navier Stokes Turbulent models; the $k-\varepsilon$ and $k-\omega$ models are used for the simulation to determine axial velocity, turbulent intensity and skin friction coefficient along the length of the pipe. The Reynolds number based on the pipe diameter and average velocity at the inlet is 10,000. The fluid used for this purpose is air and the pipe material is aluminium. The results obtained computationally are compared with experimental data and shows that using the $k-\varepsilon$ model gives more compatible results with

those obtained from experiments.

Keywords: *Computational fluid dynamics, Reynold's Averaged Navier Stokes, Turbulent intensity, Axial Velocity, Skin friction Coefficient.*

Nomenclature

C_f	Skin friction coefficient
D	Diameter of Pipe, m
I	Turbulent intensity
L	Length of Pipe, m
$\hat{n}$	Outward normal at the surface.
P	Pressure
R	Radius of pipe, m
Re	Reynolds number
S	Surface of the control volume
U	Mean velocity
V	Cell volume $[m^{-3}]$
$\vec{v}$	Velocity vector $[ms^{-1}]$
v	Velocity at the inlet m/s.
τ_w	Wall shear stress
ρ	Density of fluid kg/m^3
u'	Root-mean-square of the turbulent velocity fluctuations
μ	Dynamic viscosity
∇	Gradient operator
τ	Shear stress $[Nm^{-2}]$

ε Turbulent dissipation [$m^2 s^{-3}$]

k Turbulent kinetic energy [$m^2 s^{-2}$]

ω Specific dissipation [s^{-1}]

1. Introduction.

All flows encountered in engineering practice become unstable above a certain Reynolds number. At low Reynolds number flows are laminar. At higher Reynolds number, flows are observed to become turbulent. A chaotic and random state of motion develops in which the velocity and pressure change continuously with time within substantial regions of flow. Turbulence is characterized by flow visualization as eddies, which vary in sizes from the largest to the smallest. Largest eddies contain most of the energy, which break up into successfully smaller eddies with energy transfer to yet smaller eddies until an inner scale is reached. In a turbulent flow, the velocity and other flow properties vary in a random and chaotic manner. A turbulent flow can be characterized by the mean values of flow properties and statistical properties of their fluctuations.

In industrial scale, fluid flow patterns are often turbulent and for the prediction of the process, mathematical modelling is needed. Computational fluid dynamics can simulate many processes such as turbulent combustion, heat transfer rate and radiation by using mathematical modelling. Numerical method is the basis of computational fluid dynamics and it is based on mass, energy and momentum continuity equations. First, total fluid space is divided into small components, then

the continuity differential equations for each of these components are resolved.

In this paper, the standard $k-\varepsilon$ and $k-\omega$ models were used to model flow in the studied geometry. The Standard $k-\varepsilon$ model (Launder and Spalding, 1974) model is the most widely used complete RANS model and it is incorporated in most commercial CFD codes (Tannehill J. C., Anderson D. A., Richard H. 1997). In this model, the model transport equations are solved for two turbulence quantities i.e. k and ε.The $k-\varepsilon$ turbulence model solves the flow based on the assumption that the rate of production and dissipation of turbulent flows are in near-balance in energy transfer (Ferrey P. and Aupoix B. 2006). The standard $k-\omega$ model (Wilcox, 1998) is very similar in structure to the $k-\varepsilon$ model but the variable ε is replaced by the dissipation rate per unit kinetic energy ω.

The main aim of this paper was to obtain a model which gives a better approximation to experimental results obtained from the literature.

2. Literature review

Several studies have been done on the flow patterns in pipes by Mullin T. and Peixinho J. (2006), Sahu M. *et al* (2009), Willis A. P *et al* (2008). Rudman *et al* (2002) compared results from experimental and numerical investigations of non–Newtonian fluids at transition to turbulence and in weakly turbulent flows. Experimental results showed flow features similar to turbulent puffs and slugs observed in Newtonian transitional flows. Numerical results showed some quantitative discrepancies with the experimental results but did show turbulence suppression, drag reduction and delayed transition as observed experimentally.

Yogini P. (2010) carried out a numerical simulation of flow past a circular cylinder, using a commercial CFD code (ANSYS Fluent 12.1) with large eddy simulation (LES) and RANS Shear-Stress Transport (SST) approaches for Reynolds 1000 and 3900. The numerical results extracted from these simulations have good agreement with the experimental data of Zdravkovich M.M. (1997). Analysis of fully developed turbulent flow in a pipe using computational fluid dynamics was carried out by Bhandari D. and Singh S. (2012) and the results obtained computationally were in agreement with analytical results.

3. Computational domain

The computational domain and the boundary conditions for the simulation of the flow are shown in Figure 3.1. The cylinder is simulated with a diameter (D) and length L. This paper will consider the flow inside a pipe of diameter 0.25m and a length of 20m using FLUENT 6.3.26. The geometry is symmetric therefore we will model only half portion of the pipe (radius R).

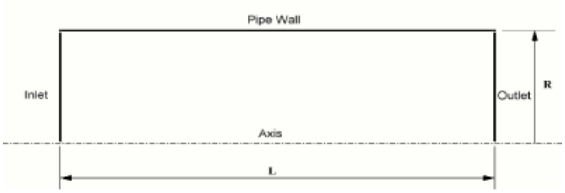

Figure 3.1: computational geometry and boundary conditions.

Air enters from the inlet boundary with a constant velocity $u = 1m/s$, density $\rho = 1$ kg/m^3 and coefficient of viscosity $\mu = 2.5 \times 10^{-5}\ kg/ms$. The fluid exhausts into

the ambient atmosphere which is at a pressure of 1 atm. The Reynolds number based on the pipe diameter and average velocity at the inlet is:

$$\mathrm{Re} = \frac{\rho u D}{\mu} = 10{,}000$$

At this Reynolds number, the flow is usually completely turbulent.

4. Governing Equations

Applying the fundamental laws of mechanics to a fluid gives the governing equations for a fluid. The conservation of mass equation is

$$\frac{\partial \rho}{\partial t} + \nabla \cdot \left(\rho \vec{V} \right) = 0 \tag{1}$$

and the conservation of momentum equation is

$$\rho \frac{\partial \vec{V}}{\partial t} + \rho \left(\vec{V} \cdot \nabla \right) \vec{V} = -\nabla p + \rho \vec{g} + \nabla \cdot \tau_{ij} \tag{2}$$

These equations along with the conservation of energy equation form a set of coupled, nonlinear partial differential equations. It is not possible to solve these equations analytically for most engineering problems. However, it is possible to obtain approximate computer-based solutions of the governing equations for a variety of engineering problems. In this investigation, simulation of turbulent flow in a pipe has been done by FLUENT v6.3.26, which uses finite volume approach in which the integral form of the conservation equations are applied to the control volume defined by a cell to get the discrete equations for the cell. The integral

form of the continuity equation for steady incompressible flow is

$$\int_S \vec{V} \cdot \hat{n}\, dS = 0 \tag{3}$$

The integration is over the surface S of the control volume and $\hat{n}$ is the outward normal at the surface. Physically, this equation means that the net volume flow into the control volume is zero.

5. Simulation set-up

The analysis is carried out with the help of CFD package FLUENT 6.3.26. Geometry and grid generation is done in GAMBIT 2.3.16 which is the preprocessor bundled with FLUENT.

In this 2D-code, a steady and pressure based solver is used. A least square cell based method is used to calculate gradients. Boundary conditions and the discretization schemes used are summarized in Table 1 below. We have considered convergence criteria 1.0×10^{-6} for these simulations.

Table 5.1: Simulation settings for flow in a pipe with RANS models

Settings	Choice
Simulation type	2D, Steady
Space	Axisymmetric
Solver	Double precision, pressure based, and implicit
Temporal discretization	2^{nd} order
Turbulence model	$k-\varepsilon$ / $k-\omega$ model
Pressure	Standard
Pressure-velocity coupling	SIMPLE
Momentum	2^{nd} order upwind
Turbulent kinetic energy	2^{nd} order upwind
Turbulent dissipation rate (for $k-\varepsilon$ model)	2^{nd} order upwind
Specific dissipation rate (for $k-\omega$ model)	2^{nd} order upwind
Convergence criteria	$1x10^{-6}$
Boundary conditions:	
Inlet	Velocity inlet
Outlet	Pressure outlet
Top wall	No-slip wall
Bottom wall	Axis

6. Results and Discussion

Here all simulations have been done using a grid which contains 6000 quadrilateral cells. Characteristics of the simulation in this case are summarized below;

```
Grid Size

Level    Cells    Faces    Nodes   Partitions
    0     6000    12160     6161            1

 1 cell zone, 5 face zones.
```

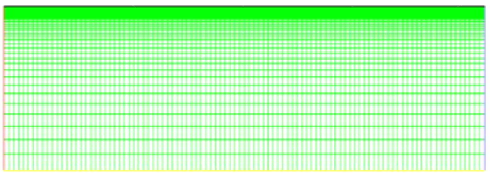

Figure 6.1: Constructed mesh of studied geometry

Numerical results were obtained for the two models for velocity, skin friction coefficient and Turbulent Intensity along the length of the pipe as shown below:

Axial velocity

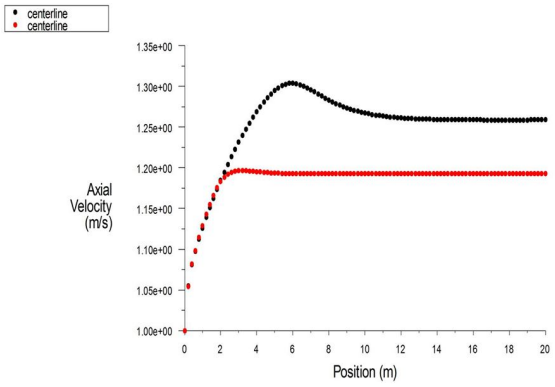

Figure 6.2: Axial velocity along the centerline of the pipe for $k-\varepsilon$ model (red) and $k-\omega$ model (black)

In figure 6.2, the velocity reaches a constant value beyond a certain distance from the inlet at x=2m and x = 6m respectively. This is the fully-developed flow region where the centerline velocity becomes a constant. As the flow develops downstream of the inlet, the viscous boundary layer grows, and will eventually fill the pipe completely (provided that the tube is long enough). When this happens, the flow becomes fully developed and there is no variation of the velocity profile in the axial direction.

Plotting the velocity at the outlet as a function of the distance from the center of the pipe gives the following results:

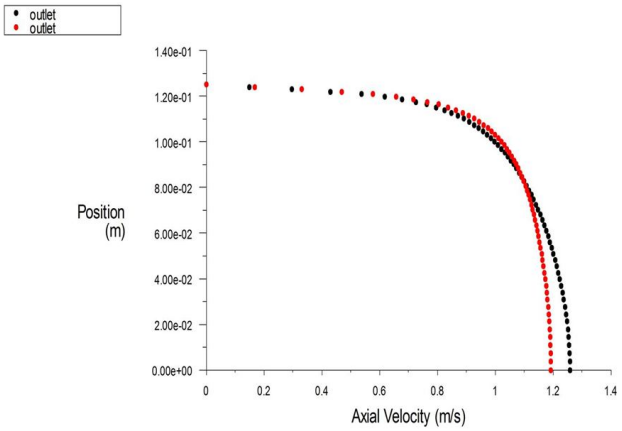

Figure 6.3: Velocity Profile at the outlet from center of the pipe for $k-\varepsilon$ model (red) and $k-\omega$ model (black)

The axial velocity profiles in Figure 6.3 for both models show a similar trend. They have a flattened shape at the wall corresponding to zero velocity. The vector magnitudes are minimum at the wall and increase towards the centerline .This is in agreement with no-slip condition along the wall and higher velocities at the centerline for conservation of mass. When a fluid is bounded by a solid surface, molecular interactions cause the fluid in contact with the surface to seek momentum and energy equilibrium with that surface. All fluids at the point of contact take on the velocity of that surface. Fluid adjacent to the wall sticks to the wall due to friction effect. The eddy motion loses its intensity close to the wall and diminishes at the wall because of the no-slip condition.

Skin Friction Coefficient

Skin Friction Coefficient is a non-dimensional parameter defined as the ratio of the

wall shear stress and the reference dynamic pressure

$$C_f \equiv \frac{\tau_w}{\frac{1}{2}\rho v^2} \tag{6.1}$$

Where τ_w is the wall shear stress, and ρ and v are the fluid density and velocity at the inlet respectively.

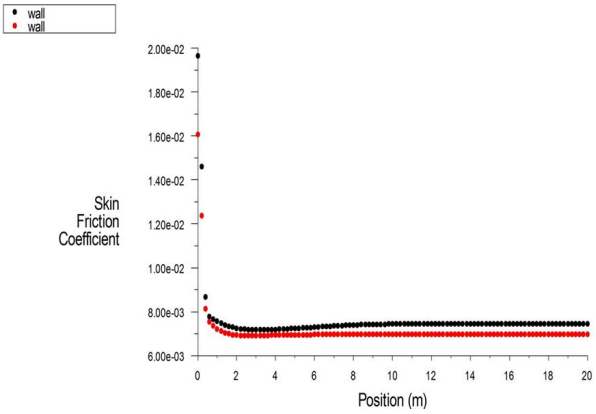

Figure 6.4: Skin Friction coefficient along the top wall for $k-\varepsilon$ model (red) and $k-\omega$ model (black)

In figure 6.4 for both models, the values at the inlet are much higher and C_f profiles have similar shape all along the length of the pipe. The wall shear stress is the highest at the pipe inlet where the thickness of the boundary layer is smallest and decreases gradually to the fully developed value. Therefore the pressure drop is higher in the entrance region of a pipe resulting in large velocity gradients and consequently larger wall shear stress.

Turbulent Intensity

The turbulence intensity, also often referred to as turbulence level, is defined as:

$$I = \frac{u'}{U} \tag{6.2}$$

Where u' is the root-mean-square of the turbulent velocity fluctuations and U is the mean Velocity.

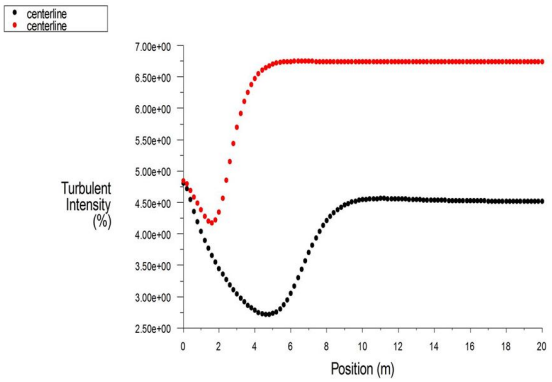

Figure 6.5: Turbulent Intensity along the centerline for $k-\varepsilon$ model (red) and $k-\omega$ model (black)

The turbulent intensities show a decrease at the inlet for both models up to some distance; the first 2m and 6m for the $k-\varepsilon$ and $k-\omega$ models respectively. After these distances there is a rapid increase and the intensity goes beyond the set value of 5% for the $k-\varepsilon$ model. This decrease in turbulent intensity corresponds to an increase in velocity (figure 6.2)

7. Conclusion

When compared with experimental results, the centerline velocity for the fully developed region according to figure 6.2 is 1.19m/s with $k-\varepsilon$ model while the experimental results show a value of 1.22m/s. The $k-\omega$ gives a value of 1.26m/s. The results for the first model are closer to the experimental value.

For fully developed turbulent flow of air, the value of skin friction coefficient comes out to be 0.01 while values obtained computationally are 0.0063 and 0.007 for the $k-\varepsilon$ and $k-\omega$ respectively (figure 6.4. The $k-\omega$ has a better prediction for the skin friction coefficient.

The turbulent intensities show a decrease at the inlet for both models but the prediction of the $k-\varepsilon$ model has significant variation away from the inlet compared to experimental value of 5% (figure 6.5). However it can be seen that a decrease in turbulent intensity corresponds to an increase in velocity.

It is also observed from the results that the axial velocity against position of centerline reveal that the axial velocity increases along the length of the pipe and after some distance it becomes constant which is in conformity with the results obtained experimentally. The axial velocity is maximum at the centerline and zero at the wall to satisfy the no-slip boundary condition for viscous flow

The results of the skin friction coefficient against the wall also reveal that it decreases along the length of the pipe with maximum being at the inlet which is in conformity with experimental results.

References

[1] Bhandari D. and Singh S. (2012). Analysis of fully developed turbulent flow in a pipe using computational fluid dynamics. International Journal of Engineering Research & Technology.Vol. 1, 2278-0181, 2012

[2] Ferrey P. and Aupoix B. (2006). Behaviour of turbulence models near a turbulent/non turbulent interface revisited, Journal of Heat and Fluid Flow, Vol.27, p. 831-837.

[3] Launder B. E. and Spalding D. B. (1972). Mathematical models of turbulence, Departments of Mechanical Engineering, Imperial College of Science and Technology, London, England

[4] Mullin T. and Peixinho J. (2006). Transition to Turbulence in pipe flow, Journal of Low Temperature Physics, 145, 75-88.

[5] Rudman M., Graham L. J., Blackburn H. M., Pullum L. *Non-Newtonian Turbulent and Transitional Pipe Flow.* Presented at Hy15, Banff, Canada, 2002

[6] Sahu M., Khatua K. K. ,Kanhu C. P. and Naik T., Developed laminar flow in pipe using computational fluid dynamics, 2009, 7th International R & D Conference on Development and Management of Water and Energy Resources, 4-6 February 2009, Bhubaneswar, India

[7] Tannehill J. C., Anderson D. A., Richard H., (1997). Computational fluid mechanics and heat transfer, Second addition, Taylor and Francis, London

[8] Wilcox D.C. (1998).Turbulence modeling for CFD, DCW Industries, Inc., La Canada, California.

[9] Willis A. P, Peixinho J., Kerswell R.R., Mullin T. (2008). Experimental and theoretical progress in pipe flow transition, Phil. Trans. Roy.Soc A 366, 2671-2684

[10] Yogini Patel (2010) Numerical Investigation of Flow Past a Circular Cylinder and in a Staggered Tube Bundle Using Various Turbulence Models. *M.Sc* Lappeenranta University of Technology

[11] Zdravkovich, M. M., (1997). Flow around circular cylinders Vol 1: fundamentals, First edition. Printed in Oxford University Press, New York.

BIOGRAPHY

Bathsheba Menge

Bathsheba Menge is a lecturer at Technical University of Mombasa ,department of Mathematics and Physics; has a B.Ed from Kenyatta University (1989) , MSc. Applied Mathematics (2002) from Kenyatta University; and is currently persuing her ph.D in Applied Mathematics Jomo Kenyatta University of Agriculture and Technology.